ORIGINAL ARTICLE

The big star of the Hawaiian Islands and scale invariance of the tectonic stars

Roberto Spina

Spina R. The big star of the Hawaiian Islands and scale invariance of the tectonic stars. J Environ Geol. 2018;2(S1):3-18.

ABSTRACT

The Hawaiian Islands and the surrounding seabed are affected by volcano-tectonic phenomena that generate particular star-shaped morphologies. The term "scale invariance" indicates the similarity of the mechanisms, regardless of the scale considered, leading to the formation of particular radial structures with symmetry inversely proportional to their sizes. The images of the seabed show, at the small scale [4-12 Km], seastar-shaped structures with a high degree of symmetry, even if their regularity is often fragmented by the gregarious character of the stars. Similar forms are repeated even on medium scales [several tens of kilometers] with structures characterized by less symmetry due to crustal anisotropy, developing in three-dimensional form. Surprisingly, the same morphologies is also confirmed on large scales [hundreds of kilometers]: more than a hundred tectonic-volcanic structural elements alternate radially around the southernmost part of the Hawaii-Emperor chain indicating, directly and indirectly, the presence of deep tectonic structures due to thermal swelling, typical of hotspot areas. Among the structures identified the longest are the pockmark trains, developed for more than 500 Km and perfectly recognizable thanks to the good resolution of the images. The grouping and interactions between tectonic stars, which dislocate their arms, are further phenomena characterized by scale invariance. The discovery of the big hawaiian star could reveal, in the near future, interactions between radial structures even on a large scale.

Key Words: *Hawaii islands; Big star; Volcano-tectonic; Star-shaped tectonic structures; Pockmark trains; Radial structures; Kilauea rift system*

In the different parts of the world, pockmarks, in addition to playing the role of markers to define some important geological phenomena [presence of oil and gas hydrates] and precursors of high magnitude seismic events have also, in some cases, an important structural significance: their presence is able to give useful information on structural elements not directly observable in outcrop. Pockmarks dimension ranging in size from the 'unit pockmark' [1 m-10 m wide, <0.6 m deep] to the normal pockmark [10 m-700 m wide, up to 45 m deep] are known to occur in most seas, oceans, lakes and in many diverse geological settings (1).

The pockmarks may be aligned along a specific direction [pockmark trains] and may be paleochannel markers (2-4) or indicators of buried tectonic structures (5,6). Pockmark trains are associated with areas of steeper seabed gradient: Pinet N et al. (2), have identified a 15 Km long pockmark trains, consisting of 109 aligned pockmarks, that show a complete transition from well-defined, relatively deep [up to 8.6 m], crater-like depressions to subtle, partly buried morphological features.

Recently particular radial arrangements of the pockmarks, known as pockmark stars, have been found in the surrounding seafloors of the Hawaiian Islands, characterized by a high degree of symmetry similar to the sea star structure. These shapes have variable dimensions in a range of about 4-12 kilometers. Their genesis can be explained by a swelling of the topographic surface, which generates a series of fractures that radiate from the maximum point of curvature, due to the buoyancy of the underlying magma chamber. A significant feature of these particular volcano-tectonic morphologies is the gregarious nature: they often develop one next to the other or overlap, generating transcurrent dislocations (7).

The high density of the stars and their location close to the hotspot of Hawaii raises questions about the existence of similar tectonic-volcanic mechanisms able to replicate these phenomena even at medium and large scales.

The swelling of the topographic surface, one of the phenomena previously mentioned, is a recurring process even at large scale due to the magmatic underplating existing in many areas of hotspots. King SD and Adam C (8), analyzed swell geometry [width and height] and buoyancy flux for 54 hotspots using the latest and most accurate data, although a significant uncertainty persist in calculation of buoyancy fluxes, with those of the Pacific in general larger than for Eurasian, North American, African and Antarctic hotspots. Considering the data obtained from previous studies of the past, the estimate of swell heights ranged from 500 m-1,200 m and swell width's ranged from 1,000 Km-1,500 Km with an estimated accuracy of roughly ± 200 m (9).

Gravimetric surveys showed weak positive anomalies in areas surrounding the Hawaiian Islands. These experimental data are in agreement with the swelling phenomenon that has weakly raised a large region extended for about 400 Km [Hawaiian swell]. In this way there has been a magma ascent that has accumulated in the areas close to the earth's surface generating a weak excess of gravity around the Hawaiian chain that has fed consistent lava flows (10).

The growth of the Hawaiian swell, connected to the hotspot's intraplate volcanism, would promote associated extensional stress, especially to the east, ahead of the active volcanic locus. This regional hotspot-related uplift could counterbalance subsidence of the oceanic crust due to isostatic adjustment accompanying loading by the enormous Hawaiian volcanoes (11).

Another widely discussed question concerns the relationships between submarine tectonic structures connected to the dynamics of volcanic edifices. Similarly to the pockmark stars, even the radial structures present in the Hawaiian islands, represented by the volcanic apparatuses, are often developed in close contact with each other and affected by active rifting phenomena that extend outward from the summits for 100 Km or more (12). An example is the island of Hawai'i where there are rift areas in the volcanoes of Mauna Loa [SW and NE rift zones] and Kilawea [SW and E rift zones]. These rift zones grow preferentially upward and outward to the seaward side, spreading laterally on a décollement formed along the interface between the volcanic edifice and the seafloor (13,14). The processes of volcano growth migrate rift-zone flanks seaward and are associated with a cyclic evolution of flank instability. The mechanisms of seaward flank migration involve all of the basic structural elements of Hawaiian volcanoes and provide clues to promising paths for future research (13).

There are additional rift processes that extend for several kilometers in the Hawaiian offshore (Figure 1), which have generated submarine ridges [Puna,

National Order of Geologists, Rome, Italy

Correspondence: Spina R, Geologist and D Comp Science, National Order of Geologists, Rome, Italy. Telephone +39 340 2545644, e-mail robertospina@geologi.it
Received: June 28, 2018, Accepted: August 30, 2018, Published: September 12, 2018

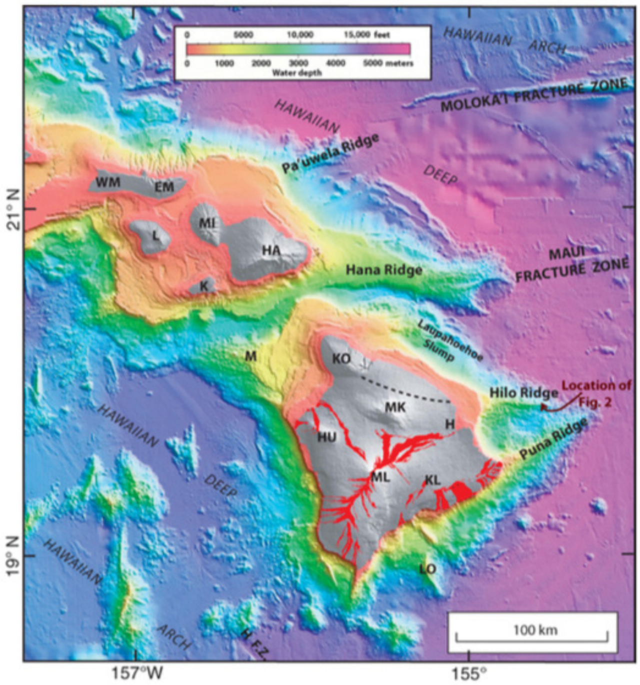

Figure 1) *Bathymetric map showing locations of long submarine rift zones. Historical eruptions in red. Dashed line is inferred buried east rift of Kohala. Volcanoes: EM - East Molokai'i; HA - Haleakala; HU - Hualalai; K - Kaho'olawe; KL - Kilauea; KO - Kohala; L - Lanai; LO - Lo'ihi; M - Mahukona; MI - West Maui; MK - Mauna Kea; ML - Mauna Loa; WM - West Molokai'i. H - Hilo [site of Hawaii Scientific Drilling Project hole]; HF.Z. - Hawaii Fracture Zone [north end only]. Modified from Robinson et al (16)*

Hilo, Hana]. They are due to the prolongation of the volcanic apparatus from which they derive:

i. Puna ridge is considered the offshore extension of Kilauea's east rift zone (15).

ii. Hana ridge is considered the offshore extension of Haleakala east rift zone and has a considerable length (16).

iii. Hilo ridge is closest to Mauna Kea but isotopical data consider it likely to be a rift zone of the volcano Kohala (17).

The reconstruction of this latter submarine structure is quite controversial. The submarine Hilo Ridge has been interpreted as a part of Mauna Kea volcano, but Holcomb RT et al. (18), found that it is crossed at ~1100 m depth by a submerged shoreline terrace composed of basalts that are isotopically distinct from those of Mauna Kea and similar to those of Kohala volcano. This terrace evidently is a product of Kohala instead of Mauna Kea. Almost all of Hilo Ridge below the terrace therefore must predate the principal growth of Mauna Kea, which has superficially isolated the ridge from its Kohala source by overlapping its proximal segment (Figure 2). Similar overlaps are suspected among other volcanoes and may cause significant changes in the understanding of Hawaiian volcanism.

Walter TR and Amelung F (19), after examining the historic eruption and earthquake catalogues of the Hawaii area have demonstrate the hypothesis that the events are interconnected in time and space. Earthquakes in the Kaoiki area occur in sequence with eruptions from the NERZ [Northeast Rift Zone], and earthquakes in the Kona and Hilea areas occur in sequence with eruptions from the SWRZ [Southwest Rift Zone]. Using three-dimensional numerical models, they demonstrate that elastic stress transfer can explain the observed volcano-earthquake interaction.

Other submarine rift zones are represented by Ka'ena ridge [a submerged remnant of the ancient shield Kaena volcano] and Penguin bank [prolongation of the west-southwest rift of west Molokai volcano].

The analyzed bibliographic data provide indications on the existence of topographic swelling processes, volcano associations with radial structures and volcano-tectonic interactions of their rift zones, coinciding with their respective flanks. These phenomena are in many ways unclear and still under discussion.

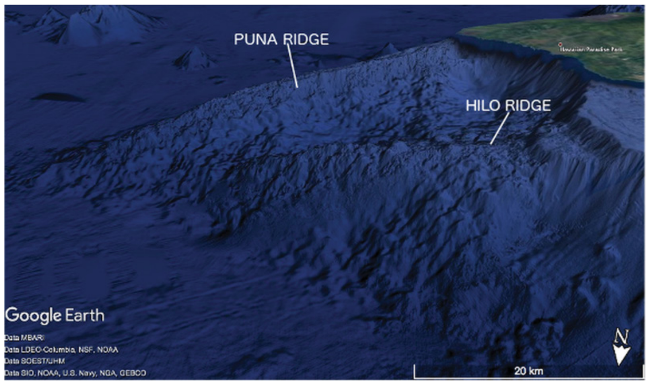

Figure 2) *Interaction between Puna and Hilo Ridge*

The problem that arises is the possible existence of a macro radial structure that can support the hypothesis of a replica, at large scales, of the processes that at smaller scales have generated sea-star shapes in the seabed of the Hawaiian Islands. In such a situation also the phenomena of clustering and interaction could be part of the same evolutionary phylum of radial structures that manifests itself at different scales.

Under these prerogatives the main objective of this work is to identify structural elements present in the seabed circumscribed by the Hawaiian swelling that can provide useful information on mechanisms and processes that have determined the evolutionary pattern of the Hawaii Islands.

METHODS

With the aid of bathymetric images [Google Earth Pro version 7.3.1.4507], the seabed surrounding the southernmost part of the Hawaii-Emperor chain [islands of Hawa'i, Maui, Kaho'olawe, Lana'i, Moloka'i, O'ahu, Kaua'i, Ni'ihau, Kaho'olawe] was analyzed. The use of some tools available in Google Earth Pro [line for measuring distances and direction on a straight, path for the measurement of distances on a broken, altitude profile] has allowed to be calculated the length, direction and the coordinates of some structural elements represented by: Linear Pockmark Trains [LPT],Volcanic Rift Zone [VRZ], Submarine Ridge [SR], Morphological Discontinuities [MD], Bands of Pockmarks and Volcanic Dikes [BPVD].

For each structural element, the geographic coordinates and alignment directions, expressed in decimal degrees, were sampled. To define the azimuth of each structural alignment we referred to the progradation direction from the convergence zone supposed as origin and coinciding, depending on the case, with one or more previously listed islands.

To establish whether there is a correlation between two qualitative or quantitative characters x_i and y_i of the same statistical unit the bivariate analysis was used.

Consider the statistical variables x and y: it is possible to represent, through a double-input data table, the distribution of the frequencies of their modes $\{x_1, x_2, \ldots x_n\}$ and $\{y_1, y_2, \ldots y_n\}$ in order to associate to each pair (x_i, y_i) the corresponding absolute frequency, called joint frequency. As a modality of the variable y the different structural elements aligned along specific directions were considered and as a mode of the variable x the alignment directions of the structural elements, in increments of 20° in the interval 0°-360°. The double entry table allowed to calculate marginal frequencies of the variables x and y corresponding to the totals of each row and column that represent the distributions of the two characters considered individually.

Using the marginal distributions of the frequencies of the double-input data table, the table of theoretical independence frequencies has been created, to define whether the two statistical variables are correlated or not. Each element of the table is recalculated through the product of the corresponding marginal frequency divided by the number of data n: $f_{i,j} = (f_{i,0} \times f_{0,j})/n$. In this way, as a new value for each cell (i, j), the joint frequency $f_{i,j}$ is considered.

If the table obtained coincides perfectly with the initial one the two variables are independent, otherwise they are correlated with one another.

RESULTS

The satellite observation carried out in the seabed surrounding the most advanced part of the Hawaii-Emperor chain reveals the existence of particular alignments of structural elements of different types. In particular:

- Linear Pockmark Trains [LPT] correspond to sequences of pockmarks that develop linearly according to specific directions, up to distances of about 500 Km.
- Volcanic Rift Zone [VRZ] specifies the axes of the active rift systems in the islands belonging to the Hawaiian chain.
- Submarine Ridge [SR] indicate submarine mountainous complexes consisting of volcanic ridges generally connected to fracturing zones [Moloka'i Fracture Zone, Maui Fracture Zone, Horizon tablemount, Clark seamount,..]. Diapiric ridge are also included in this category.
- Morphological Discontinuities [MD] indicate a topographic variation of the seabed [from a few tens to hundreds of meters] of uncertain origin. In some cases, based on observations, they could be due to lavic channels or fractures/faults.
- Band of Pockmarks and Volcanic Dikes [BPVD] indicate a portion of the seabed, between 1 Km and 10 Km wide, colonized by pockmarks, transversal fractures and volcanic dikes. In some cases the density of these structural elements is very high and provides a high contrast with the contiguous areas of the seafloor, tectonically less disturbed.

Table 1 shows the characteristics of each alignment with the geographic coordinates corresponding to the starting point, the structural elements present, the direction of development and the length in kilometers. Table 2 shows the directions of the arms of about fifty pockmark stars, calculated starting from the point of convergence of each star, whose position corresponds to the geographic coordinates present.

On the whole there is a radial star structure with the different arms [more than a hundred] that converge at the Hawaiian Islands. The diagram in Figure 3A identifies each alignment with a specific number, corresponding to that shown in Table 1. This sequence of structural elements draws particular geometries referring to relict forms and/or evolutionary processes in progress. In some cases linear development includes only elements belonging to a specific category while, in other cases, there is a mixture of different structural elements [for example linear pockmark train-submarine ridge associations] prograding along the same direction. In the same image, different types of structural elements are defined by specific colors shown in the legend. Figure 3B shows the location of the images and topographic profiles performed on different arms.

Figure 4A shows a succession of pockmarks that develop linearly, for a good 430 Km, in the 193° direction [arm 47]. Thanks to the high resolution of the images produced by Google Earth, the linear development of the pockmark train is perfectly recognizable along its entire length. Figure 4B shows that the same succession of pockmarks converges on the western side of the island of O'ahu. Figure 4C indicates that the sequence of pockmarks also goes up the steep escarpment of the island of O'ahu [on the left indicated with the number 1]. On the right, the number 2 indicates the ascent of a pockmark train that corresponds to the coalescence of two successions of pockmarks [arms 46 and 47] with the latter developed for 384 Km.

In Figure 5A we can observe another pockmark train [arm 124] that develops, towards the eastern side of the Hawaiian Islands, for a total length of 400 Km. Figure 5B shows a topographic profile along the pockmarks axis. In Figure 6 a linear pockmark train extends toward the western side of the Hawaiian chain [arm 61] and connects with the submarine ridge [arm 60] which continues in the same direction. The arrow in figure indicates the connection zone between the two structural elements. In Figure 7A a top view of two bands of pockmaks and volcanic dikes [arms 98 and 99], with an average width of 6 Km and developed towards the island of Hawaii for about 120 Km. In the image of Figure 7B a close vision of band 2: it can be noted the high density of pockmarks and volcanic dikes present within the band. Figures 8A and 8B [arm 108] show respectively a top and bottom view of a submarine ridge developed on a band of pockmark and volcanic dikes. It can be noted that the upper part of the ridge is strongly articulated by the presence of pockmarks and dikes. In Figures 9A and 9B a top and close view of a succession of small volcanic dikes alternated with pockmarks [arm 34], both developed towards the Hawaiian Islands. Figures 10A and 10B show a morphological discontinuity due to a rise in the sea floor [arm 72]: on the back it is possible to observe, in line with the previous structure, a submarine

TABLE 1

Arms of the big star (Hawaii islands)

Arm	Longitude	Latitude	Direction	Length (Km)	Type of structure
1	-155.679333°	18.891828°	200°	35	Volcanic Rift Zone
2	-155.289006°	18.989536°	157°	29	Volcanic Rift Zone
3	-154.798464°	19.527659°	59°	71	Volcanic Rift Zone
4	-154.925859°	19.867266°	89°	46	Volcanic Rift Zone
5	-155.883082°	20.273812°	329°	25	Volcanic Rift Zone
6	-156.330087°	20.066304°	286°	41	Volcanic Rift Zone
7	-156.074265°	19.728519°	322°	45	Volcanic Rift Zone
8	-155.958093°	20.714153°	106°	110	Volcanic Rift Zone
9	-155.333602°	20.631298°	84°	64	Volcanic Rift Zone
10	-156.053723°	21.233581°	70°	40	Volcanic Rift Zone
11	-156.709723°	20.524221°	254°	73	Volcanic Rift Zone
12	-157.787953°	21.046084°	181°	52	Volcanic Rift Zone
13	-157.611732°	21.306672°	109°	11	Volcanic Rift Zone
14	-157.984000°	21.733124°	349°	24	Volcanic Rift Zone
15	-158.514709°	21.794654°	322°	48	Volcanic Rift Zone
16	-158.283042°	21.575323°	300°	75	Volcanic Rift Zone
17	-159.411201°	21.852839°	167°	19	Volcanic Rift Zone
18	-159.304261°	22.217566°	29°	32	Volcanic Rift Zone
19	-159.582159°	22.261316°	356°	54	Volcanic Rift Zone
20	-159.909001°	22.158953°	302°	52	Volcanic Rift Zone
21	-159.795593°	22.015917°	235°	29	Volcanic Rift Zone
22	-160.260295°	21.900808°	300°	31	Volcanic Rift Zone
23	-160.280384°	21.805222°	239°	25	Volcanic Rift Zone
24	-160.632985°	21.670688°	277°	23	Volcanic Rift Zone
25	-160.531632°	21.639313°	147°	16	Volcanic Rift Zone
26	-158.790260°	21.265819°	272°	333	Linear Pockmark Trains
27	-164.409918°	21.395218°	249°	392	Submarine Ridge
28	-168.488756°	20.320501°	240°	99	Submarine Ridge
29	-167.546213°	19.992415°	244°	289	Submarine Ridge
30	-166.368518°	20.272409°	244°	190	Submarine Ridge
31	-160.719094°	21.002530°	257°	223	Submarine Ridge
32	-161.765344°	20.595930°	280°	261	Submarine Ridge

33	-164.853750°	20.023702°	253°	120	Submarine Ridge
34	-159.693030°	20.616733°	247°	222	Band of Pockmark and Volcanic Dikes
35	-160.882172°	19.986504°	250°	287	Submarine Ridge
36	-161.398297°	19.699036°	255°	332	Submarine Ridge
37	-162.753898°	19.262408°	255°	113	Submarine Ridge
38	-158.703671°	20.786044°	237°	44	Submarine Ridge
39	-158.367746°	20.717053°	218°	100	Linear Pockmark Trains
40	-159.005234°	20.069966°	271°	39	Linear Pockmark Trains
41	-159.488570°	19.989647°	256°	500	Submarine Ridge
42	-163.120000°	18.762749°	251°	36	Submarine Ridge
43	-158.873566°	19.633601°	286°	76	Submarine Ridge
44	-158.857094°	19.697016°	183°	48	Submarine Ridge
45	-158.229261°	20.399882°	202°	144	Linear Pockmark Trains
46	-158.119293°	20.361048°	202°	217	Linear Pockmark Trains -Submarine Ridge
47	-158.005431°	20.808079°	193°	430	Linear Pockmark Trains
48	-157.699209°	20.645520°	169°	22	Submarine Ridge
49	-157.607545°	20.112904°	182°	47	Submarine Ridge
50	-157.262943°	19.520799°	207°	36	Submarine Ridge
51	-157.558521°	19.272221°	222°	66	Submarine Ridge
52	-158.156414°	18.839673°	216°	50	Submarine Ridge
53	-158.456986°	18.450733°	183°	22	Submarine Ridge
54	-157.159022°	19.289851°	171°	122	Submarine Ridge
55	-157.081781°	18.666666°	207°	49	Submarine Ridge
56	-157.310336°	18.273677°	246°	41	Submarine Ridge
57	-157.655402°	18.127366°	154°	143	Submarine Ridge
58	-157.630577°	17.680221°	168°	163	Submarine Ridge
59	-157.102153°	19.625613°	158°	79	Submarine Ridge
60	-157.186612°	20.187922°	165°	28	Submarine Ridge
61	-157.082176°	19.898578°	149°	90	Linear Pockmark Trains
62	-156.725283°	19.736399°	167°	34	Submarine Ridge
63	-156.867126°	17.832055°	189°	55	Submarine Ridge
64	-156.567969°	18.327648°	180°	144	Band of Pockmark and Volcanic Dikes
65	-156.271354°	18.789905°	205°	36	Submarine Ridge
66	-156.030107°	19.000247°	184°	28	Submarine Ridge
67	-155.952870°	18.779352°	178°	27	Submarine Ridge
68	-156.411676°	18.487213°	180°	161	Band of Pockmark and Volcanic Dikes
69	-156.233316°	18.338477°	184°	66	Band of Pockmark and Volcanic Dikes
70	-156.156827°	18.194889°	185°	53	Morphological Discontinuities
71	-156.212749°	17.754641°	183°	82	Submarine Ridge
72	-156.092274°	18.154787°	182°	74	Band of Pockmark and Volcanic Dikes
73	-156.056990°	18.222324°	180°	75	Submarine Ridge
74	-155.933610°	18.478054°	180°	96	Band of Pockmark and Volcanic Dikes
75	-155.968367°	17.156287°	199°	118	Submarine Ridge
76	-155.762655°	17.896856°	180°	99	Band of Pockmark and Volcanic Dikes
77	-155.643596°	17.755359°	180°	82	Band of Pockmark and Volcanic Dikes
78	-155.474585°	17.721257°	181°	81	Band of Pockmark and Volcanic Dikes
79	-155.329620°	17.559489°	177°	62	Band of Pockmark and Volcanic Dikes
80	-155.155192°	17.398713°	181°	43	Band of Pockmark and Volcanic Dikes
81	-156.385421°	18.466075°	131°	185	Morphological Discontinuities
82	-155.947376°	18.502609°	180°	42	Band of Pockmark and Volcanic Dikes
83	-155.743031°	18.489502°	183°	56	Linear Pockmark Trains
84	-155.566834°	18.040448°	150°	35	Morphological Discontinuities
85	-155.550680°	18.068391°	150°	54	Morphological Discontinuities
86	-155.196713°	17.987770°	197°	26	Morphological Discontinuities
87	-155.268558°	17.763866°	158°	23	Morphological Discontinuities
88	-155.184038°	17.925901°	199°	18	Morphological Discontinuities
89	-155.160224°	18.084683°	179°	48	Band of Pockmark and Volcanic Dikes
90	-155.152484°	17.652477°	167°	26	Morphological Discontinuities
91	-154.989893°	18.180813°	180°	120	Band of Pockmark and Volcanic Dikes
92	-155.754697°	18.625307°	106°	53	Submarine Ridge
93	-154.970192°	18.435589°	110°	218	Band of Pockmark and Volcanic Dikes
94	-154.748150°	18.531614°	106°	170	Band of Pockmark and Volcanic Dikes
95	-155.007392°	18.659264°	105°	218	Band of Pockmark and Volcanic Dikes
96	-155.322745°	19.181943°	137°	20	Submarine Ridge
97	-153.987802°	19.013148°	93°	65	Submarine Ridge
98	-154.289852°	20.174104°	89°	134	Band of Pockmark and Volcanic Dikes
99	-154.138416°	20.333866°	90°	118	Band of Pockmark and Volcanic Dikes
100	-154.145623°	20.475525°	90°	118	Band of Pockmark and Volcanic Dikes
101	-154.094693°	20.636334°	90°	112	Band of Pockmark and Volcanic Dikes

102	-153.539948°	20.761666°	86°	375	Submarine Ridge
103	-154.047246°	20.840305°	87°	435	Submarine Ridge
104	-152.447192°	20.974928°	88°	270	Submarine Ridge
105	-155.004851°	21.072118°	88°	95	Band of Pockmark and Volcanic Dikes
106	-154.021506°	21.057992°	89°	105	Band of Pockmark and Volcanic Dikes
107	-155.001326°	21.277895°	89°	246	Submarine Ridge
108	-155.005033°	21.366027°	87°	275	Submarine Ridge
109	-154.915815°	21.413051°	85°	509	Submarine Ridge
110	-154.977884°	21.458213°	84°	350	Submarine Ridge
111	-155.177476°	21.538470°	88°	117	Submarine Ridge
112	-152.843851°	21.743696°	78°	302	Submarine Ridge
113	-155.376085°	21.596556°	82°	241	Submarine Ridge
114	-154.276230°	21.778969°	78°	125	Submarine Ridge
115	-154.551671°	21.812790°	76°	483	Submarine Ridge
116	-157.109149°	21.664306°	80°	43	Submarine Ridge
117	-156.947622°	21.802471°	68°	31	Submarine Ridge
118	-156.762658°	22.165030°	116°	34	Linear Pockmark Trains
119	-157.074247°	21.993619°	327°	20	Submarine Ridge
120	-155.461791°	22.878589°	72°	285	Submarine Ridge
121	-157.381187°	22.059950°	21°	98	Linear Pockmark Trains
122	-156.375331°	23.407355°	84°	52	Submarine Ridge
123	-152.990765°	23.994558°	72°	60	Submarine Ridge
124	-156.813251°	23.487542°	74°	400	Linear Pockmark Trains
125	-156.991098°	23.733556°	102°	65	Submarine Ridge
126	-155.798805°	23.793412°	75°	112	Submarine Ridge
127	-158.924950°	23.511321°	85°	100	Submarine Ridge
128	-157.375390°	23.977402°	81°	197	Submarine Ridge
129	-154.265859°	24.602163°	72°	127	Submarine Ridge
130	-155.680689°	24.379799°	64°	198	Submarine Ridge

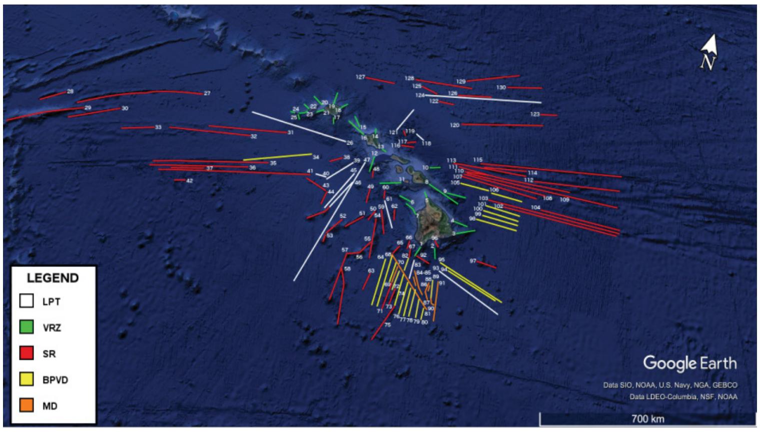

3(A)

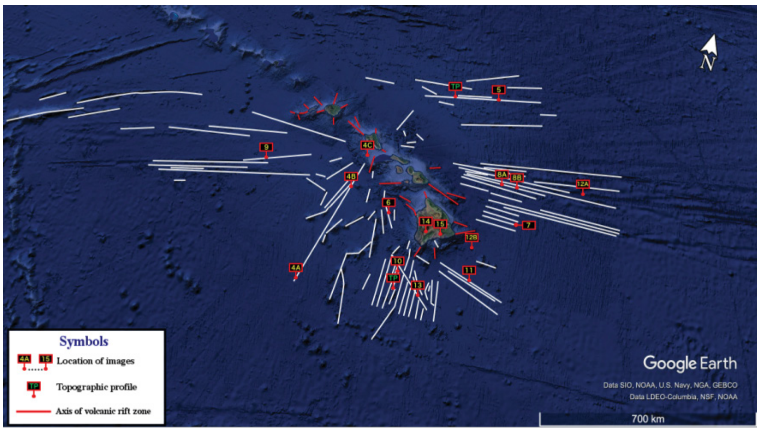

3(B)

Figure 3) *Distribution of the big star's arms. For a description of each arm [type, coordinates of the start point and length] refer to Table 1A. The numbers indicate the arms and colors the different structural elements that make them up. Acronyms: LPT - linear pockmark trains;SR – submarine ridge; VRZ - volcanic rift zone; MD - morphological discontinuities; BPVD - bands of pockmarks and volcanic dikes. B) Location of photos and topographic profiles performed on the different arms*

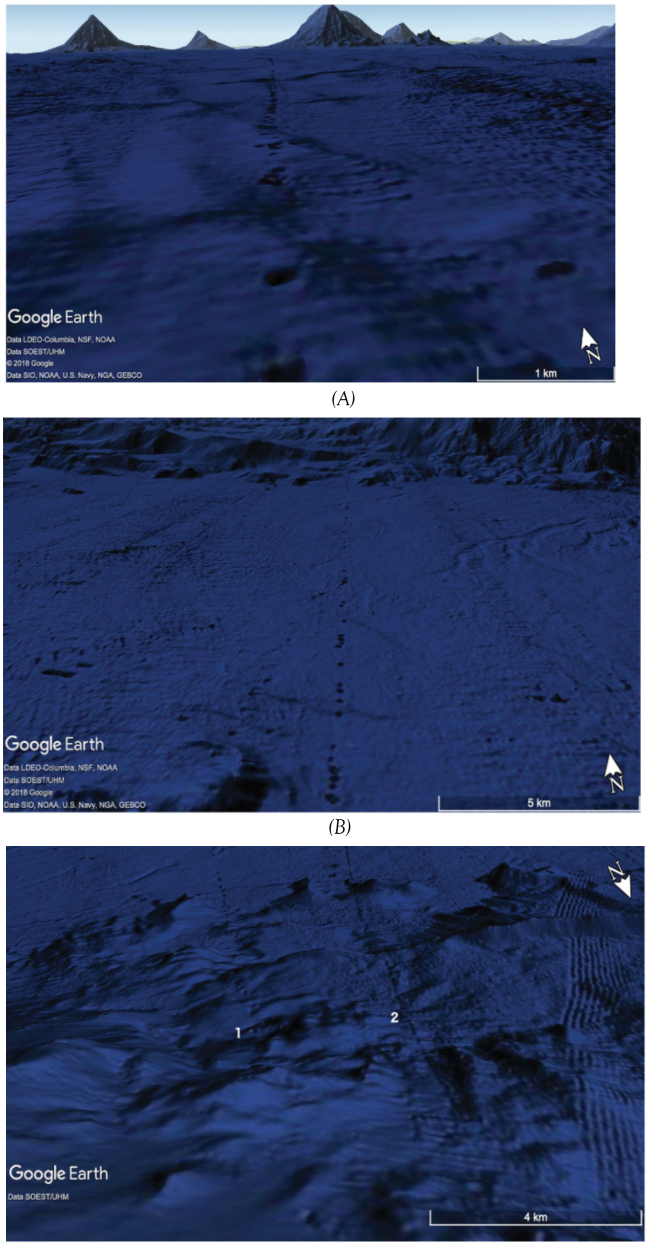

Figure 4) *Linear pockmark train, about 430 Km long, converging into the Hawaii islands [western sector]. A) Terminal part of the pockmark train. B) The previous structure near the island of O'ahu. C) Ascent of the linear pockmark train [indicated with the number one] in the escarpment of the O'ahu island*

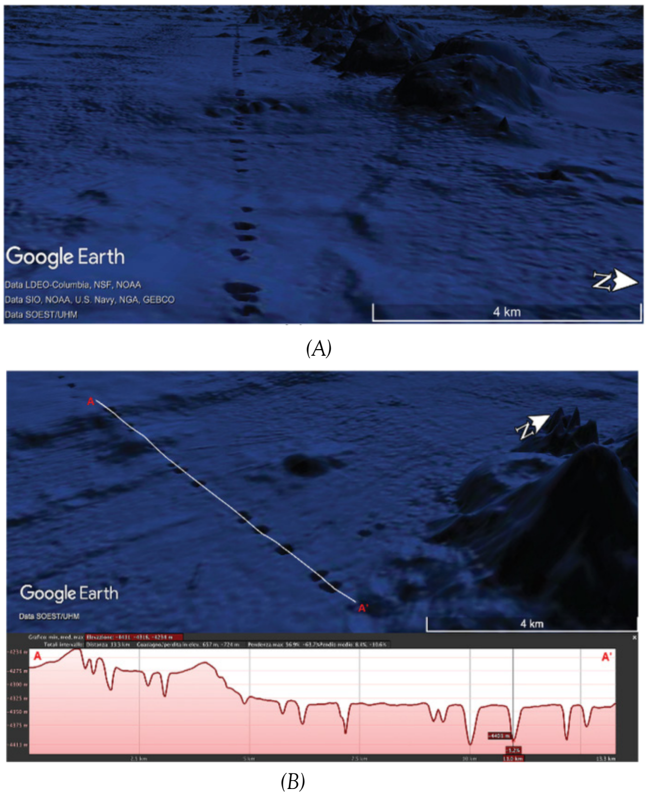

Figure 5) *Linear pockmark trains, about 400 Km long, converging into the Hawaii islands [eastern sector]. A) Longitudinal view. B) Longitudinal topographic profile*

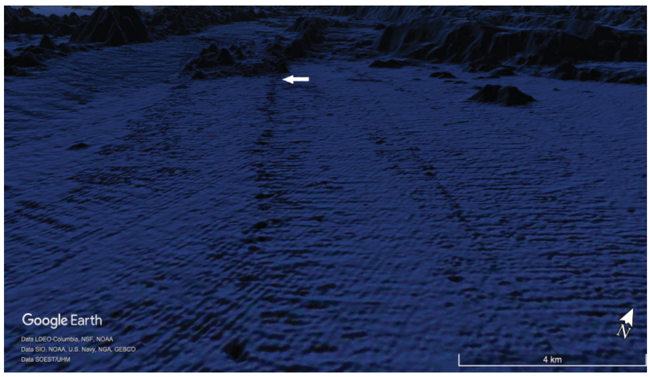

Figure 6) *Transition from a succession of pockmarks to a submarine ridge. The arrow indicates the passage zone*

ridge. Figure 11 shows a succession of transverse fractures aligned in the direction of the island of Hawaii [arm 95]: the images show that the genesis of these particular fractures is due to the coalescence of individual pockmarks elongated transversely to the direction of development. In Figure 12A it is possible to observe the development of a convergent submarine ridge in the eastern sector of the Hawaiian Islands. In Figure 12B convergence towards Hawaii affects several submarine ridge: the arrow indicates the position of the previous view. In Figures 13A and 13B [arm 81] a top and close view of a morphological discontinuity of the seabed which interrupts the continuity of a series of the bands of pockmark and volcanic dikes [arms 68 to 80]. Figures 14 and 15 show three different sinkhole sequences present in the flanks of the Mauna Loa volcano. The images show a close correspondence between these structures and the pockmarks trains (shown in white in Figure 3A) identified in the seabed surrounding the Hawaiian islands. Two details of the previous image are shown in Figure 14B and 14C: in Figure 14B the sinkholes go up a small volcanic cone, while in Figure 14C the formation of the elongated depression (indicated by the arrow) is due to the coalescence of contiguous sinkholes. Figure 15 shows two distinct sinkhole sequences (indicated by numbers 1 and 2) placed at a distance of about 800 m from each other, with the sinkhole train 2 which tends to reconnect to the previous one.

Two rose charts were made on the basis of the data in Table 1 and Table 2, divided into 18 classes, on the 0°-360° scale at intervals of 20°. For each class the absolute frequency has been represented with circular sectors proportional to it. In this way it was possibile to analyze the type of distribution of the structural elements associations and any similarities with small-scale stars. The aim is to establish whether there is a similarity between the orientation of the small stars [length of the arms between 4 and 12 Km] present in the seabed proximal to the Hawaii islands and the arms of the big Hawaiian star [length of the arms up to 500 Km].

In the first case the rose diagram shows a bilateral symmetry (Figure 16A) with the highest frequency values included in the 0°-80° and 180°-260° intervals. In the second case there is a less symmetrical distribution (Figure 16B) with two main peaks (intervals 80°-100° and 180°-200°) and a secondary peak (interval 240°-260°).

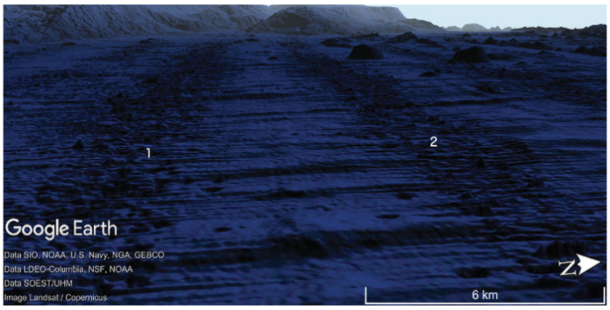

(A)

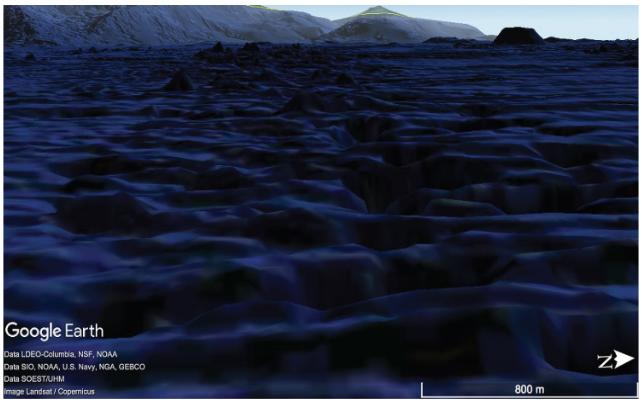

(B)

Figure 7) *Two bands of pockmaks and volcanic dikes converging in the island of Hawaii. A) View from above. The bands are indicated with the numbers 1 and 2B) Close-up view*

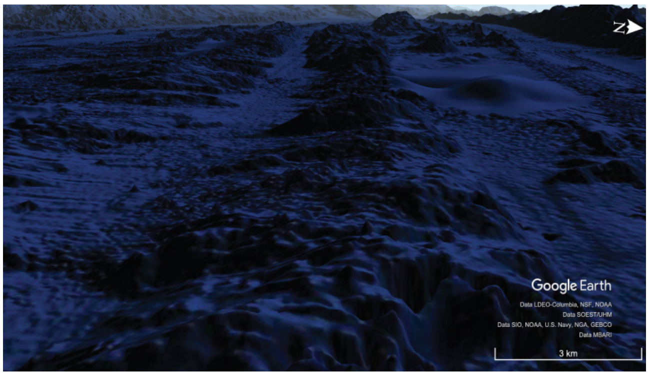

(A)

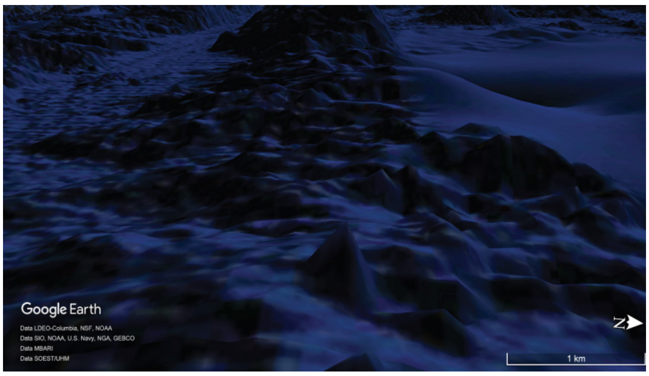

(B)

Figure 8) *Submarine ridge developed on a band of pockmark and volcanic dykes. A) View from above. B) Close-up view in which you can see the transverse ridges, the dikes and the pockmarks that make the relief considerably articulated*

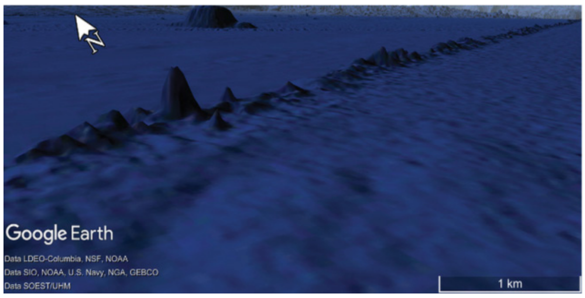

(A)

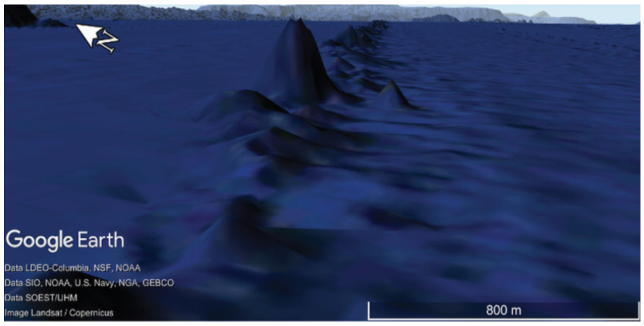

(B)

Figure 9) *Small volcanic dikes converging into the Hawaii islands [western sector]. A) Lateral view. B) Close-up view*

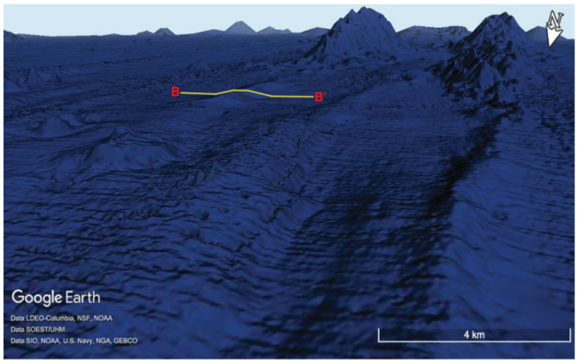

(A)

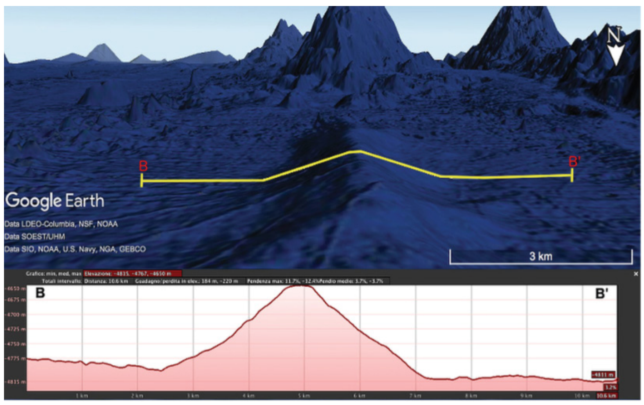

(B)

Figure 10) *Morphological discontinuity converging in the island of Hawaii. A) Aerial view. B) Transversal topographic profile. Note the passage from topographic relief to the submarine ridge [immediately behind].*

The bivariate analysis applied to the A [Alignment Direction] and B [Type of Structural Element] characters allowed to obtain a double-input data table (Figure 16C), in which to each pair (x_i, y_i) of the values of A and B corresponds to a specific absolute frequency f_{ij} [joint frequency]. Based on the marginal frequencies obtained it was possible to obtain two bar charts:

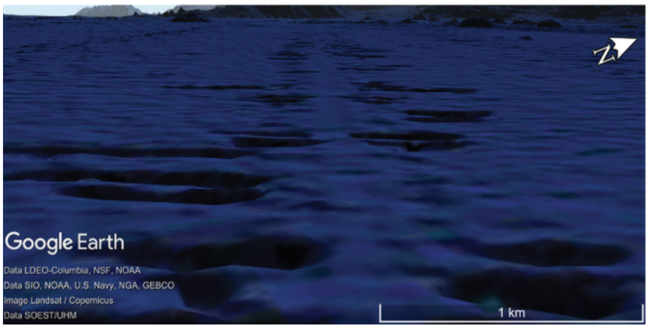

Figure 11) *Transversal fractures prograding towards the southern side of the island of Hawai'i. An in-depth analysis reveals that the structures are due to the coalescence of contiguous pockmarks.*

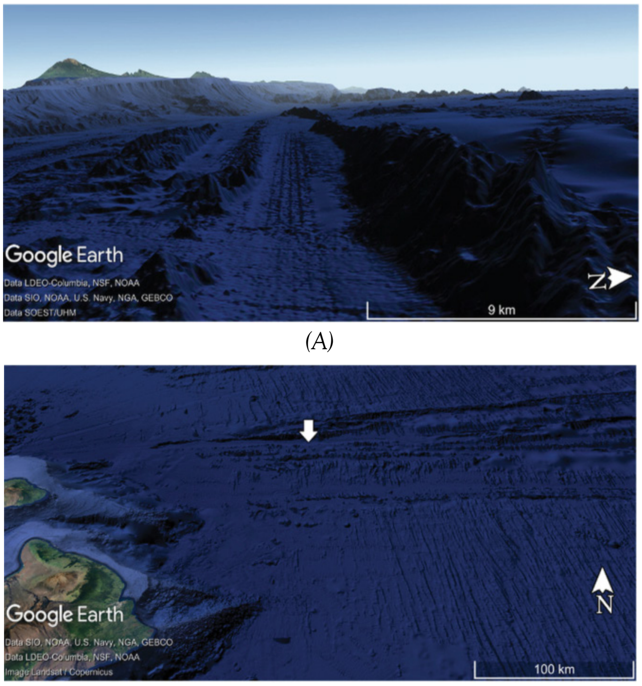

(A)

(B)

Figure 12) *Submarine ridge converging in the island of Hawaii. A) Close-up view. B) View from the southern sector of the Hawaiian Islands. Note several submarine volcanic chains that converge towards the island of Hawaii. The arrow indicates the position of the previous view*

The bar chart of Figure 16D shows the presence of a major peak corresponding to Submarine Ridge and two additional secondary peaks (Band of Pockmark and Volcanic Dikes and Volcanic Rift Zone). They therefore represent the most widespread structural elements found on the sea floor, which converge towards the Hawaiian Islands.

The bar chart of Figure 16E shows that in the interval 0°- 20° there is total absence of structures, while in the intervals 20°- 60°, 140°-160° and 260°-360° the minimal values of structural elements have been found.

Based on the double-input data table, the theoretical independence frequencies table (Figure 16F) was constructed. As can be seen, the values obtained differ considerably and, as explained above, this indicates the existence of a correlation between the two characters [A and B] considered.

DISCUSSION

The analysis of the ocean floor has revealed the existence of particular volcano-tectonic structures, with different development and orientation, which overall draw a radial geometry around the southernmost part of the Hawaiian chain, defined tectonic star. Similar to most of the star-shaped structures found in the seabed surrounding the islands (7), they converge

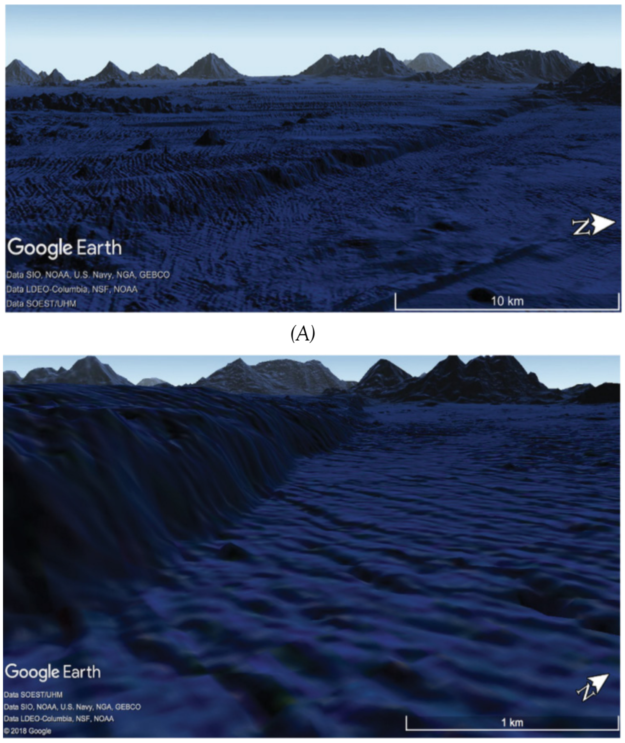

(A)

(B)

Figure 13) *Morphological discontinuity with presumable tectonic origin. The maximum difference in level is about 450 m. A) Lateral view. B) Close-up view*

in Hawaii's high structural zone. The structural elements show different characteristics that seem to be the superficial reflection of deep phenomena whose intensity also conditions the way in which they occur.

Morphological discontinuities are topographic difference in height which testifies, in a direct way, the presence of deep shear zones able to propagate for hundreds of kilometers. Submarine ridges are structures that, indirectly, presuppose the presence of deep discontinuities through which large amounts of magma go up. Band of pockmarks and volcanic dikes are wide and extended shear bands in which some of the structural elements listed above alternate. A similar evidence of active tectonic stress fields are represented by the transversal fractures that also prograde towards the Hawaiian Islands reaching 100 Km of linear development (Figure 11). Traces of the presence of deep shear structures are represented by the linear development of pockmarks of heterogeneous dimensions. Surprisingly, the pockmark trains are developed in a continuous and perfectly observable way for more than 500 km up to ascend the slope that separates the Hawaiian islands from the surrounding ocean floor.

The images included in the previous section show a remarkable resemblance with the successions of sinkhole present in the sides of the volcano Mauna Loa. It is believed that these structures, also found in other volcanoes of the Hawaiian Islands, can be attributed to a pit crater linked to the ascent of volcanic dykes. It is possible to notice some of the recurring phenomena identified in the successions of pockmarks that converge in the direction of the Hawaiian Islands:

(i) Coalescence of pockmarks (Figures 4A and Figure 14C)

(ii) Pockmarks rising on a relief (Figure 4C and Figure 14B)

(iii) Development of pockmarks on subparallel directions (Figures 4B-4C and Figure 15).

Volcanic Rift Zone is crustal sectors affected by extensive fractures associated with the development of a volcano.

These intensely fractured areas are due to the push of the underlying magma that can more easily reach the surface giving rise to volcanic activity. Generally, the axes of the rift are arranged radially with respect to the volcanoes and tend to overlap in the islands where there are more volcanic apparatuses in close contact with each other.

Overall, as can be seen from the map in Figure 3, all these structures tend

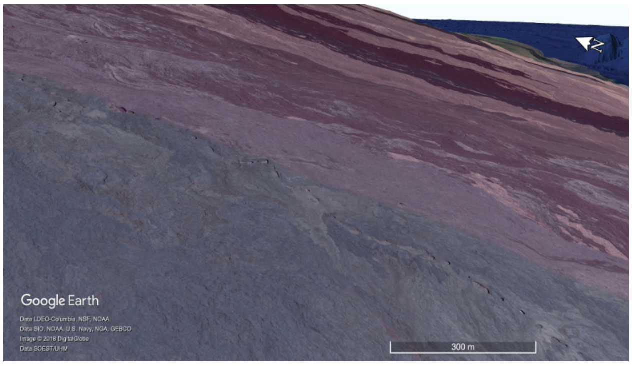

(A)

(B)

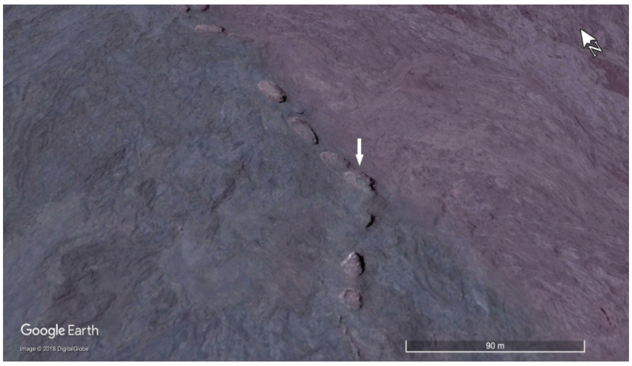

(C)

Figure 14) *Different sinkhole successions in the flanks of the Mauna Loa volcano. A) A sinkhole train that goes up the slope to the central crater. Note the perfect correspondence with the pockmark trains found in the seabed surrounding the islands of Hawaii. B) The sequence of sinkhole goes up a small volcanic cone in a manner analogous to ascent of pockmarks on seamounts. C) Coalescence of two sinkholes, indicated by the arrow, which form an elongated depression. The phenomenon has often been observed in the pockmark-based structures found in the seabed of Hawaii.*

to radiate from the island of Ni'ihaw to the island of Hawai'i, forming a "big star" for certain features similar to the small stars found in hawaiian offshore. The rose diagrams (Figures 16B and 16A) show different trends for large and small scale structures whose development methods are strongly influenced by the anisotropic characteristics of the lithosphere which tend to significantly reduce their symmetry and regularity.

Statistical analysis carried out through the theoretical independence frequencies table denotes the existence of a correlation between the alignment direction and the type of structural element. The bar chart of Figure 16D obtained considering the marginal frequencies [Number of Structural Elements/Alignment Direction] shows that the density of the structural elements depends on the direction: in some directions it is maximum, while in other directions it is minimal or absent.

Furthermore, by observing Table 1 and Figure 3A, it can be seen that in different directions of development there are transitions from one structural element to another. For example, in arm 46 we move from linear pockmark trains to submarine ridge, while in arm 74-75 we move from bands of pockmarks and volcanic dikes to submarine ridge: further transitions

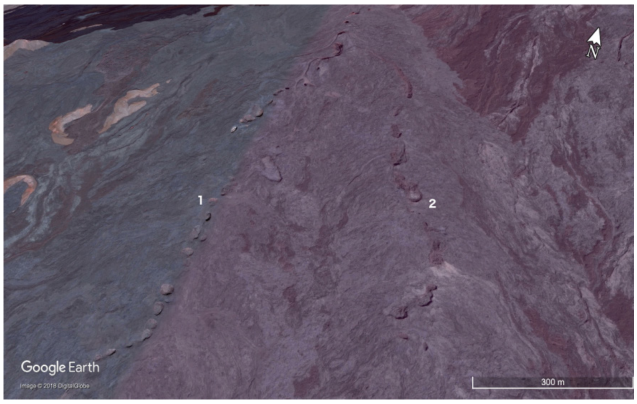

Figure 15) *Two sinkhole sequences developed a short distance from each other. Similar structures consist of pockmark were found in the Hawaiian seabed*

TABLE 2

Classification of the small star's arms [seabed surrounding the Hawaii islands]. Latitude and longitude are expressed in decimal degrees

Star	Arms	Centre of the star		Direction
		Latitude	Longitude	
S1	**1**	**19.413723°**	**-153.952389°**	**341°**
S1	2	19.413723°	-153.952389°	356°
S1	3	19.413723°	-153.952389°	193°
S1	4	19.413723°	-153.952389°	206°
S1	5	19.413723°	-153.952389°	231°
S1	6	19.413723°	-153.952389°	243°
S1	7	19.413723°	-153.952389°	257°
S1	8	19.413723°	-153.952389°	287°
S1	9	19.413723°	-153.952389°	303°
S1	10	19.413723°	-153.952389°	318°
S1	11	19.413723°	-153.952389°	345°
S1	12	19.413723°	-153.952389°	193°
S1	13	19.413723°	-153.952389°	208°
S1	14	19.413723°	-153.952389°	221°
S1	15	19.413723°	-153.952389°	230°
S1	16	19.413723°	-153.952389°	245°
S2	**1**	**19.334541°**	**-154.071379°**	**323°**
S2	2	19.334541°	-154.071379°	332°
S2	3	19.334541°	-154.071379°	349°
S2	4	19.334541°	-154.071379°	181°
S3	**1**	**19.404606°**	**-154.178684°**	**238°**
S3	2	19.404606°	-154.178684°	264°
S3	3	19.404606°	-154.178684°	345°
S3	4	19.404606°	-154.178684°	181°
S3	5	19.404606°	-154.178684°	201°
S3	6	19.404606°	-154.178684°	220°
S4	**1**	**19.490099°**	**-154.125301°**	**218°**
S4	2	19.490099°	-154.125301°	229°
S4	3	19.490099°	-154.125301°	240°
S4	4	19.490099°	-154.125301°	252°
S4	5	19.490099°	-154.125301°	263°
S4	6	19.490099°	-154.125301°	270°
S5	**1**	**19.443304°**	**-154.381356°**	**353°**
S5	2	19.443304°	-154.381356°	195°
S5	3	19.443304°	-154.381356°	218°
S5	4	19.443304°	-154.381356°	238°
S6	**1**	**19.412126°**	**-154.410468°**	**258°**
S6	2	19.412126°	-154.410468°	215°
S6	3	19.412126°	-154.410468°	202°
S6	4	19.412126°	-154.410468°	188°
S6	5	19.412126°	-154.410468°	351°
S6	6	19.412126°	-154.410468°	332°
S6	7	19.412126°	-154.410468°	319°
S7	**1**	**19.520061°**	**-154.352104°**	**217°**

S7	2	19.520061°	-154.352104°	227°
S7	3	19.520061°	-154.352104°	238°
S7	4	19.520061°	-154.352104°	245°
S7	5	19.520061°	-154.352104°	255°
S7	6	19.520061°	-154.352104°	271°
S7	7	19.520061°	-154.352104°	287°
S8	**1**	**19.612354°**	**-154.334295°**	**222°**
S8	2	19.612354°	-154.334295°	202°
S8	3	19.612354°	-154.334295°	187°
S8	4	19.612354°	-154.334295°	351°
S8	5	19.612354°	-154.334295°	336°
S8	6	19.612354°	-154.334295°	322°
S8	7	19.612354°	-154.334295°	309°
S8	8	19.612354°	-154.334295°	299°
S8	9	19.612354°	-154.334295°	286°
S8	10	19.612354°	-154.334295°	265°
S8	11	19.612354°	-154.334295°	250°
S9	**1**	**19.555820°**	**-154.327342°**	**293°**
S9	2	19.555820°	-154.327342°	287°
S9	3	19.555820°	-154.327342°	276°
S9	4	19.555820°	-154.327342°	270°
S9	5	19.555820°	-154.327342°	263°
S9	6	19.555820°	-154.327342°	259°
S9	7	19.555820°	-154.327342°	250°
S10	**1**	**19.661230°**	**-154.270045°**	**267°**
S10	2	19.661230°	-154.270045°	250°
S10	3	19.661230°	-154.270045°	234°
S11	**1**	**19.049105°**	**-154.169863°**	**325°**
S11	2	19.049105°	-154.169863°	345°
S11	3	19.049105°	-154.169863°	182°
S11	4	19.049105°	-154.169863°	200°
S11	5	19.049105°	-154.169863°	222°
S11	6	19.049105°	-154.169863°	236°
S11	7	19.049105°	-154.169863°	232°
S11	8	19.049105°	-154.169863°	214°
S11	9	19.049105°	-154.169863°	199°
S11	10	19.049105°	-154.169863°	183°
S12	**1**	**18.761444°**	**-154.137833°**	**324°**
S12	2	18.761444°	-154.137833°	336°
S12	3	18.761444°	-154.137833°	346°
S12	4	18.761444°	-154.137833°	191°
S12	5	18.761444°	-154.137833°	201°
S12	6	18.761444°	-154.137833°	211°
S12	7	18.761444°	-154.137833°	220°
S12	8	18.761444°	-154.137833°	235°
S12	9	18.761444°	-154.137833°	192°
S12	10	18.761444°	-154.137833°	203°
S12	11	18.761444°	-154.137833°	214°
S12	12	18.761444°	-154.137833°	223°
S13	**1**	**18.778831°**	**-154.166002°**	**348°**
S13	2	18.778831°	-154.166002°	184°
S13	3	18.778831°	-154.166002°	196°
S13	4	18.778831°	-154.166002°	209°
S13	5	18.778831°	-154.166002°	222°
S13	6	18.778831°	-154.166002°	234°
S13	7	18.778831°	-154.166002°	244°
S13	8	18.778831°	-154.166002°	242°
S13	9	18.778831°	-154.166002°	229°
S13	10	18.778831°	-154.166002°	219°
S13	11	18.778831°	-154.166002°	208°
S13	12	18.778831°	-154.166002°	199°
S13	13	18.778831°	-154.166002°	186°
S14	**1**	**18.878602°**	**-154.128873°**	**256°**
S14	2	18.878602°	-154.128873°	243°
S14	3	18.878602°	-154.128873°	228°
S14	4	18.878602°	-154.128873°	215°
S14	5	18.878602°	-154.128873°	214°
S14	6	18.878602°	-154.128873°	230°
S14	7	18.878602°	-154.128873°	244°
S14	8	18.878602°	-154.128873°	254°
S15	**1**	**19.764998°**	**-154.174975°**	**223°**
S15	2	19.764998°	-154.174975°	213°
S15	3	19.764998°	-154.174975°	203°
S15	4	19.764998°	-154.174975°	188°
S15	5	19.764998°	-154.174975°	181°
S15	6	19.764998°	-154.174975°	276°
S15	7	19.764998°	-154.174975°	261°
S15	8	19.764998°	-154.174975°	251°
S16	**1**	**19.908651°**	**-154.163178°**	**264°**
S16	2	19.908651°	-154.163178°	251°
S16	3	19.908651°	-154.163178°	236°
S16	4	19.908651°	-154.163178°	217°
S16	5	19.908651°	-154.163178°	200°
S16	6	19.908651°	-154.163178°	183°
S16	7	19.908651°	-154.163178°	344°
S16	8	19.908651°	-154.163178°	330°
S17	**1**	**19.949511°**	**-154.071826°**	**190°**
S17	2	19.949511°	-154.071826°	219°
S17	3	19.949511°	-154.071826°	234°
S17	4	19.949511°	-154.071826°	244°
S17	5	19.949511°	-154.071826°	256°
S17	6	19.949511°	-154.071826°	268°
S17	7	19.949511°	-154.071826°	282°
S17	8	19.949511°	-154.071826°	299°
S17	9	19.949511°	-154.071826°	309°
S18	**1**	**19.850041°**	**-153.921552°**	**194°**
S18	2	19.850041°	-153.921552°	202°
S18	3	19.850041°	-153.921552°	210°
S18	4	19.850041°	-153.921552°	215°
S18	5	19.850041°	-153.921552°	221°
S18	6	19.850041°	-153.921552°	240°
S18	7	19.850041°	-153.921552°	250°
S19	**1**	**19.643770°**	**-153.924865°**	**341°**
S19	2	19.643770°	-153.924865°	350°
S19	3	19.643770°	-153.924865°	356°
S19	4	19.643770°	-153.924865°	183°
S19	5	19.643770°	-153.924865°	187°
S19	6	19.643770°	-153.924865°	193°
S19	7	19.643770°	-153.924865°	199°
S20	**1**	**20.159701°**	**-154.405129°**	**259°**
S20	2	20.159701°	-154.405129°	246°
S20	3	20.159701°	-154.405129°	231°
S23	**1**	**20.603621°**	**-154.499094°**	**186°**
S23	2	20.603621°	-154.499094°	200°
S23	3	20.603621°	-154.499094°	219°
S23	4	20.603621°	-154.499094°	231°
S23	5	20.603621°	-154.499094°	243°
S23	6	20.603621°	-154.499094°	253°
S23	7	20.603621°	-154.499094°	260°
S23	8	20.603621°	-154.499094°	200°
S23	9	20.603621°	-154.499094°	215°
S23	10	20.603621°	-154.499094°	229°
S23	11	20.603621°	-154.499094°	239°
S26	**1**	**20.000306°**	**-154.567493°**	**318°**
S26	2	20.000306°	-154.567493°	331°
S26	3	20.000306°	-154.567493°	343°
S26	4	20.000306°	-154.567493°	356°
S26	5	20.000306°	-154.567493°	185°
S26	6	20.000306°	-154.567493°	200°
S26	7	20.000306°	-154.567493°	216°
S27	**1**	**20.130972°**	**-154.609089°**	**230°**
S27	2	20.130972°	-154.609089°	224°
S27	3	20.130972°	-154.609089°	211°
S27	4	20.130972°	-154.609089°	193°
S27	5	20.130972°	-154.609089°	358°
S27	6	20.130972°	-154.609089°	347°
S27	7	20.130972°	-154.609089°	337°
S27	8	20.130972°	-154.609089°	322°

S27	9	20.130972°	-154.609089°	311°
S27	10	20.130972°	-154.609089°	303°
S27	11	20.130972°	-154.609089°	287°
S27	12	20.130972°	-154.609089°	275°
S28	**1**	**20.096277°**	**-153.916643°**	**350°**
S28	2	20.096277°	-153.916643°	186°
S28	3	20.096277°	-153.916643°	204°
S28	4	20.096277°	-153.916643°	221°
S28	5	20.096277°	-153.916643°	237°
S28	6	20.096277°	-153.916643°	249°
S28	7	20.096277°	-153.916643°	263°
S33	**1**	**23.154571°**	**-156.857962°**	**344°**
S33	2	23.154571°	-156.857962°	353°
S33	3	23.154571°	-156.857962°	185°
S33	4	23.154571°	-156.857962°	195°
S33	5	23.154571°	-156.857962°	208°
S33	6	23.154571°	-156.857962°	219°
S33	7	23.154571°	-156.857962°	228°
S33	8	23.154571°	-156.857962°	236°
S33	9	23.154571°	-156.857962°	244°
S35	**1**	**24.749742°**	**-157.324113°**	**192°**
S35	2	24.749742°	-157.324113°	205°
S35	3	24.749742°	-157.324113°	224°
S35	4	24.749742°	-157.324113°	242°
S35	5	24.749742°	-157.324113°	276°
S35	6	24.749742°	-157.324113°	260°
S35	7	24.749742°	-157.324113°	242°
S35	8	24.749742°	-157.324113°	224°
S35	9	24.749742°	-157.324113°	206°
S35	10	24.749742°	-157.324113°	180°
S36	**1**	**24.568560°**	**-157.353600°**	**262°**
S36	2	24.568560°	-157.353600°	246°
S36	3	24.568560°	-157.353600°	253°
S36	4	24.568560°	-157.353600°	233°
S36	5	24.568560°	-157.353600°	245°
S36	6	24.568560°	-157.353600°	255°
S36	7	24.568560°	-157.353600°	232°
S36	8	24.568560°	-157.353600°	220°
S36	9	24.568560°	-157.353600°	220°
S36	10	24.568560°	-157.353600°	208°
S36	11	24.568560°	-157.353600°	207°
S36	12	24.568560°	-157.353600°	195°
S36	13	24.568560°	-157.353600°	192°
S36	14	24.568560°	-157.353600°	182°
S36	15	24.568560°	-157.353600°	181°
S36	16	24.568560°	-157.353600°	345°
S36	17	24.568560°	-157.353600°	346°
S36	18	24.568560°	-157.353600°	330°
S40	**1**	**23.756466°**	**-158.979915°**	**183°**
S40	2	23.756466°	-158.979915°	189°
S40	3	23.756466°	-158.979915°	210°
S40	4	23.756466°	-158.979915°	235°
S40	5	23.756466°	-158.979915°	244°
S40	6	23.756466°	-158.979915°	355°
S40	7	23.756466°	-158.979915°	183°
S40	8	23.756466°	-158.979915°	190°
S40	9	23.756466°	-158.979915°	213°
S40	10	23.756466°	-158.979915°	228°
S40	11	23.756466°	-158.979915°	235°
S40	12	23.756466°	-158.979915°	245°
S41	**1**	**22.999508°**	**-157.471771°**	**264°**
S41	2	22.999508°	-157.471771°	255°
S41	3	22.999508°	-157.471771°	242°
S41	4	22.999508°	-157.471771°	232°
S41	5	22.999508°	-157.471771°	221°
S41	6	22.999508°	-157.471771°	204°
S41	7	22.999508°	-157.471771°	194°
S41	8	22.999508°	-157.471771°	191°
S41	9	22.999508°	-157.471771°	204°
S41	10	22.999508°	-157.471771°	220°
S41	11	22.999508°	-157.471771°	231°
S41	12	22.999508°	-157.471771°	241°
S41	13	22.999508°	-157.471771°	252°
S41	14	22.999508°	-157.471771°	263°
S42	**1**	**22.373060°**	**-155.007258°**	**333°**
S42	2	22.373060°	-155.007258°	314°
S42	3	22.373060°	-155.007258°	296°
S42	4	22.373060°	-155.007258°	282°
S42	5	22.373060°	-155.007258°	270°
S43	**1**	**18.497750°**	**-153.969154°**	**282°**
S43	2	18.497750°	-153.969154°	270°
S43	3	18.497750°	-153.969154°	260°
S43	4	18.497750°	-153.969154°	249°
S43	5	18.497750°	-153.969154°	238°
S43	6	18.497750°	-153.969154°	224°
S43	7	18.497750°	-153.969154°	210°
S44	**1**	**20.131173°**	**-154.390202°**	**211°**
S44	2	20.131173°	-154.390202°	223°
S44	3	20.131173°	-154.390202°	242°
S44	4	20.131173°	-154.390202°	262°
S44	5	20.131173°	-154.390202°	276°
S44	6	20.131173°	-154.390202°	213°
S44	7	20.131173°	-154.390202°	225°
S44	8	20.131173°	-154.390202°	241°
S44	9	20.131173°	-154.390202°	257°
S50	**1**	**20.862928°**	**-159.223726°**	**269°**
S50	2	20.862928°	-159.223726°	257°
S50	3	20.862928°	-159.223726°	250°
S50	4	20.862928°	-159.223726°	242°
S50	5	20.862928°	-159.223726°	223°
S50	6	20.862928°	-159.223726°	215°
S53	**1**	**18.507284°**	**-156.908525°**	**209°**
S53	2	18.507284°	-156.908525°	193°
S53	3	18.507284°	-156.908525°	355°
S53	4	18.507284°	-156.908525°	337°
S53	5	18.507284°	-156.908525°	319°
S53	6	18.507284°	-156.908525°	302°
S53	7	18.507284°	-156.908525°	289°
S53	8	18.507284°	-156.908525°	276°
S58	**1**	**23.139316°**	**-156.714634°**	**316°**
S58	2	23.139316°	-156.714634°	337°
S58	3	23.139316°	-156.714634°	353°
S58	4	23.139316°	-156.714634°	186°
S78	**1**	**17.969554°**	**-158.216233°**	**192°**
S78	2	17.969554°	-158.216233°	199°
S78	3	17.969554°	-158.216233°	210°
S78	4	17.969554°	-158.216233°	212°
S78	5	17.969554°	-158.216233°	227°
S78	6	17.969554°	-158.216233°	248°
S78	7	17.969554°	-158.216233°	267°
S78	8	17.969554°	-158.216233°	319°
S78	9	17.969554°	-158.216233°	329°
S78	10	17.969554°	-158.216233°	334°
S80	**1**	**17.282772°**	**-156.337458°**	**189°**
S80	2	17.282772°	-156.337458°	212°
S80	3	17.282772°	-156.337458°	228°
S80	4	17.282772°	-156.337458°	188°
S80	5	17.282772°	-156.337458°	183°
S80	6	17.282772°	-156.337458°	331°
S83	**1**	**17.817424°**	**-158.486515°**	**213°**
S83	2	17.817424°	-158.486515°	226°
S83	3	17.817424°	-158.486515°	242°
S83	4	17.817424°	-158.486515°	258°
S83	5	17.817424°	-158.486515°	268°
S83	6	17.817424°	-158.486515°	286°
S83	7	17.817424°	-158.486515°	301°
S83	8	17.817424°	-158.486515°	309°
S86	**1**	**20.507588°**	**-154.584086°**	**357°**

S86	2	20.507588°	-154.584086°	184°
S86	3	20.507588°	-154.584086°	197°
S86	4	20.507588°	-154.584086°	213°
S86	5	20.507588°	-154.584086°	231°
S86	6	20.507588°	-154.584086°	247°
S86	7	20.507588°	-154.584086°	264°
S86	8	20.507588°	-154.584086°	277°
S86	9	20.507588°	-154.584086°	264°
S86	10	20.507588°	-154.584086°	249°
S86	11	20.507588°	-154.584086°	231°
S86	12	20.507588°	-154.584086°	214°
S86	13	20.507588°	-154.584086°	199°
S86	14	20.507588°	-154.584086°	184°
S87	**1**	**18.408418°**	**-156.502968°**	**191°**
S87	2	18.408418°	-156.502968°	203°
S87	3	18.408418°	-156.502968°	215°
S87	4	18.408418°	-156.502968°	226°
S87	5	18.408418°	-156.502968°	266°
S87	6	18.408418°	-156.502968°	203°
S87	7	18.408418°	-156.502968°	182°
S87	8	18.408418°	-156.502968°	224°
S87	9	18.408418°	-156.502968°	255°
S89	**1**	**18.665275°**	**-153.964557°**	**357°**
S89	2	18.665275°	-153.964557°	185°
S89	3	18.665275°	-153.964557°	195°
S89	4	18.665275°	-153.964557°	203°
S89	5	18.665275°	-153.964557°	215°
S89	6	18.665275°	-153.964557°	229°
S89	7	18.665275°	-153.964557°	241°
S89	8	18.665275°	-153.964557°	249°
S90	**1**	**23.789662°**	**-157.749118°**	**195°**
S90	2	23.789662°	-157.749118°	212°
S90	3	23.789662°	-157.749118°	228°
S90	4	23.789662°	-157.749118°	244°
S90	5	23.789662°	-157.749118°	260°
S90	6	23.789662°	-157.749118°	273°
S90	7	23.789662°	-157.749118°	285°
S90	8	23.789662°	-157.749118°	296°
S91	**1**	**24.101935°**	**-158.179008°**	**358°**
S91	2	24.101935°	-158.179008°	191°
S91	3	24.101935°	-158.179008°	202°
S91	4	24.101935°	-158.179008°	214°
S91	5	24.101935°	-158.179008°	223°
S91	6	24.101935°	-158.179008°	239°
S91	7	24.101935°	-158.179008°	248°
S91	8	24.101935°	-158.179008°	259°
S91	9	24.101935°	-158.179008°	267°
S91	10	24.101935°	-158.179008°	186°
S91	11	24.101935°	-158.179008°	191°
S91	12	24.101935°	-158.179008°	202°
S91	13	24.101935°	-158.179008°	214°
S91	14	24.101935°	-158.179008°	225°
S91	15	24.101935°	-158.179008°	235°
S91	16	24.101935°	-158.179008°	247°
S91	17	24.101935°	-158.179008°	259°

between two or more structural elements can be observed in other arms. This alternation of different structural elements could be linked to tectonic phenomena that are variable in space and time. Spatial variability may be due to two alternative and complementary mechanisms summarized in:

i. A greater depth of the fracture due to an efficient buoyancy thrust in the sectors proximal to the area of maximum curvature. In this way the discontinuity tends to reduce the depth gradually as you move away from the hotspot area

ii. Variable depth and extension of the magmatic tanks which, in some cases, are reached by tectonic dislocations producing intense surface magmatic activities.

The temporal variability can be linked to a modification of the thrust underlying the hotspot that can amplify or reduce the phenomenon. In some

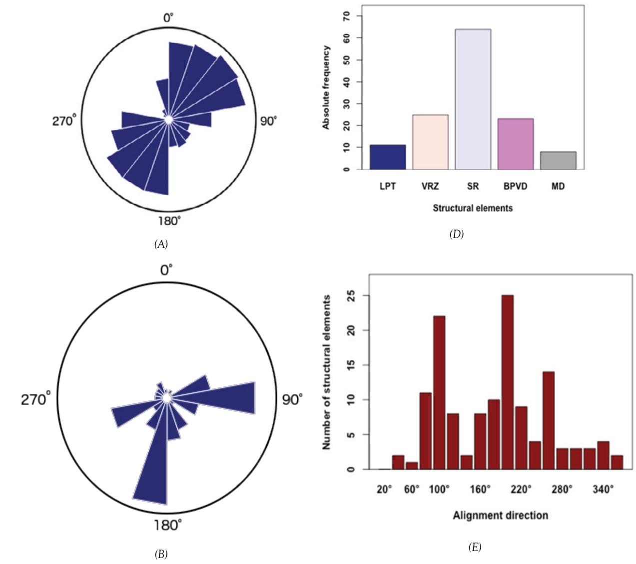

Y / X	LPT	VRZ	SR	BPVD	MD	TOTAL
20°						0
40°	1	1				2
60°		1				1
80°	1	1	9			11
100°		2	14	6		22
120°	1	2	2	3		8
140°			1		1	2
160°	1	2	2		3	8
180°		1	6	2	1	10
200°	2	1	8	11	3	25
220°	3	1	5			9
240°		2	2			4
260°		1	12	1		14
280°	2	1				3
300°		1	2			3
320°		3				3
340°		3	1			4
360°		2				2
TOTAL	11	25	64	23	8	131

(C)

Y / X	LPT	VRZ	SR	BPVD	MD	TOTAL
20°						0
40°			1			1
60°						0
80°	1	2	5	2	1	11
100°	2	4	11	4	1	22
120°	1	2	4	1		8
140°			1			1
160°	1	2	4	1		8
180°	1	2	5	2	1	11
200°	2	5	12	4	2	25
220°	1	2	4	2	1	10
240°		1	2	1		4
260°	1	3	7	2	1	14
280°		1	1	1		3
300°		1	1	1		3
320°		1	1	1		3
340°		1	2	1		4
360°			1		0	1
TOTAL	10	27	62	23	7	129

(F)

Figure 16) *Statistical analysis performed on the data in table 1 and 2. A) Rose diagram of the small star's arms - Seabed surrounding the Hawaii islands (20). B) Rose diagram of the big star's arms - Hawaii islands (20). C) Bivariate analysis represented by double-input data table [Type of structural elements/Alignment direction]. D) Bar chart of the marginal frequencies [Absolute Frequency/ Structural Elements]. E) Bar chart of the marginal frequencies [Number of Structural Elements/Alignment Direction]. F) Table of theoretical independence frequencies [Type of Structural Elements/ Alignment Direction].*

cases the original form of magmatic intrusion similar to a "pancake" can change over millions of years producing rotations of the convergence area with radial fractures that overlap the previous but characterized by different directions. The push of the hotspot can therefore occur in a polyphasic way determining, in the course of millions of years, a deepening of the tectonic discontinuities always greater.

The model in Figure 17A shows the initial magmatic pancake-shaped intrusion at the crust-mantle passage. The buoyancy produces draping of the upper crustal levels generating a slight swelling with extensive crustal fractures in the seabed that radiate from the point of maximum curvature of the pancake. Figure 17B shows the evolution of the phenomenon: from the base of the lithosphere it detaches a plume that reaches the crust and feeds an intense surface volcanic activity. Similarly to the previous case, the thrust of the most superficial magma chamber creates a curvature of the emission zone and the formation of radial structures in the shape of a star superimposed on the previous larger extension. In Figure 17C it can be seen that the surface activity leads to the construction of a volcanic apparatus whose lithostatic load creates a consistent flexure of the crust [the size of the volcano are oversized with respect to the topographic swelling]. The development of the volcanic island involves an additional load that counterbalances the buoyancy of the surface magma chamber. When the weight of the volcanic island prevails on the buoyancy force, the magma is pushed sideways with respect to the "depocentre" of the deep magma chamber. During the period of lateral spread of the magma the central activity decreases significantly

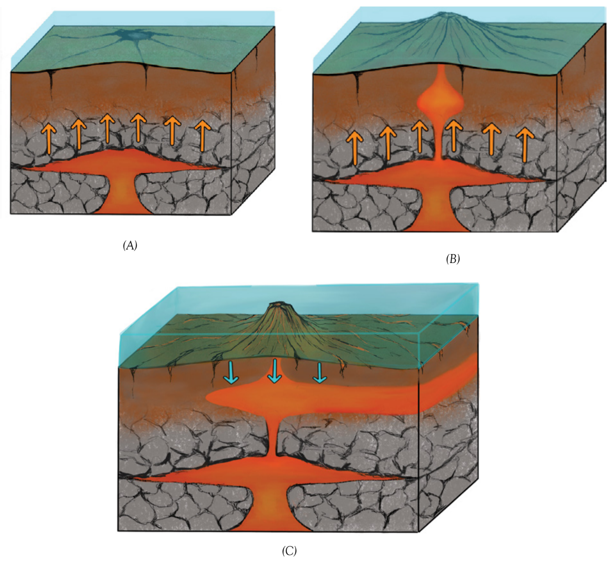

Figure 17) *Scheme of the formation process of the Hawaiian islands. A) Hospot induces a weak swelling of the crust which begins to fracture radially starting from the area of maximum curvature. B) A plume detaches from the pancake and feeds an intense volcanic activity on the surface with the crust that is arched locally: it generates a swelling with a greater radius of curvature and less extensive than the previous case. A star geometry is developed superimposed on the previous "big star". C) A volcanic edifice rises from the bottom of the sea and the increase in the lithostatic load is counterbalanced by the buoyancy of the magma. When the weight of the volcanic apparatus is greater than the buoyancy force, the magma is pushed sideways to the magma chamber [realized by Spina M]*

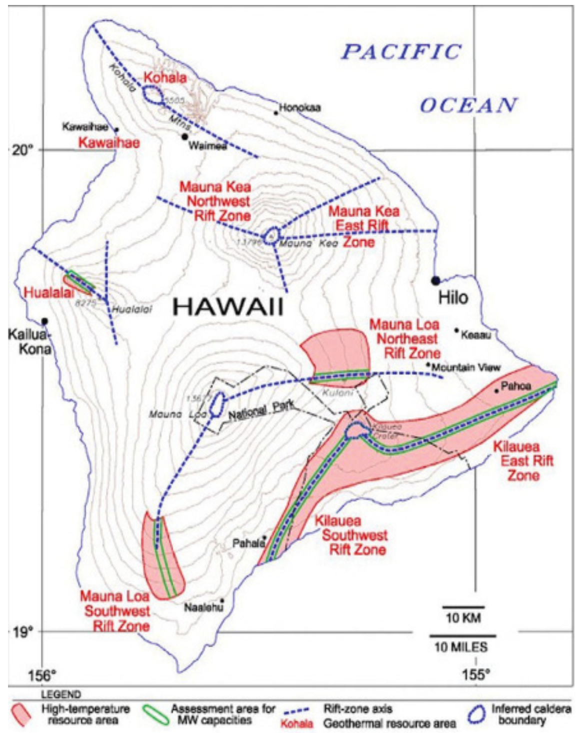

Figure 19) *Schematic of the rift zones inside the Hawai'i Island (18)*

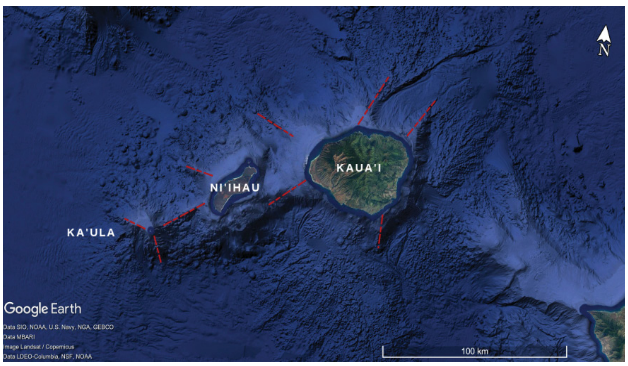

(A)

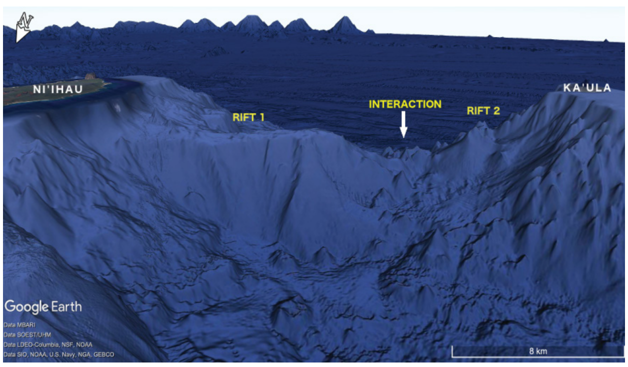

(B)

Figure 18) *An extract from the geological map of the Hawaiian islands (21). A) Tectonic structures present in the islands of the Hawaiian chain. B) Detailed view of the distribution of the axes of the rift zones [in red dotted lines] present in the Ni'ihau and Ka'ula islands. The perfect radial symmetry and the areas of interaction between contiguous stars should be noted*

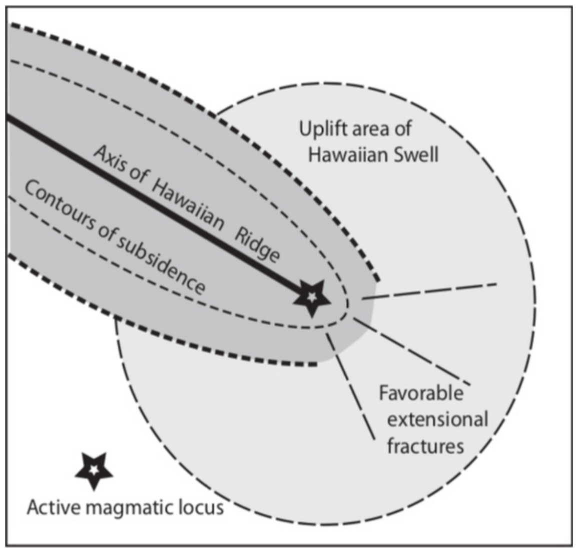

Figure 20) *Schematic interaction between uplift of Hawaiian Swell [light gray] and submergence along Hawaiian Ridge [dark gray] (17)*

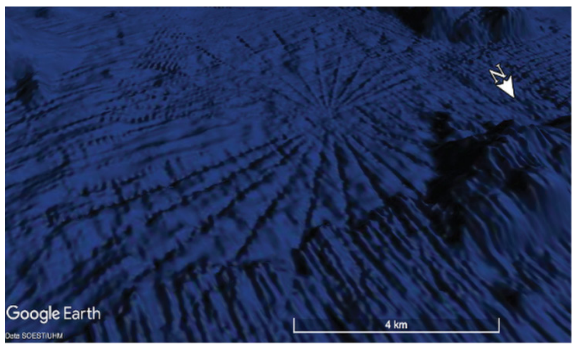

Figure 21) *Small-scale star with a high degree of symmetry*

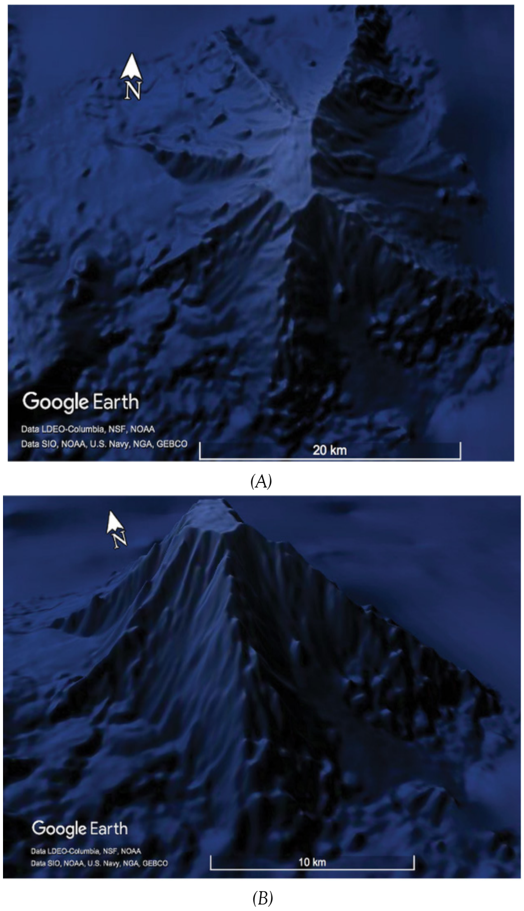

Figure 22) *Medium-scale stars with three-dimensional arms. A) Aerial view; B) Lateral view*

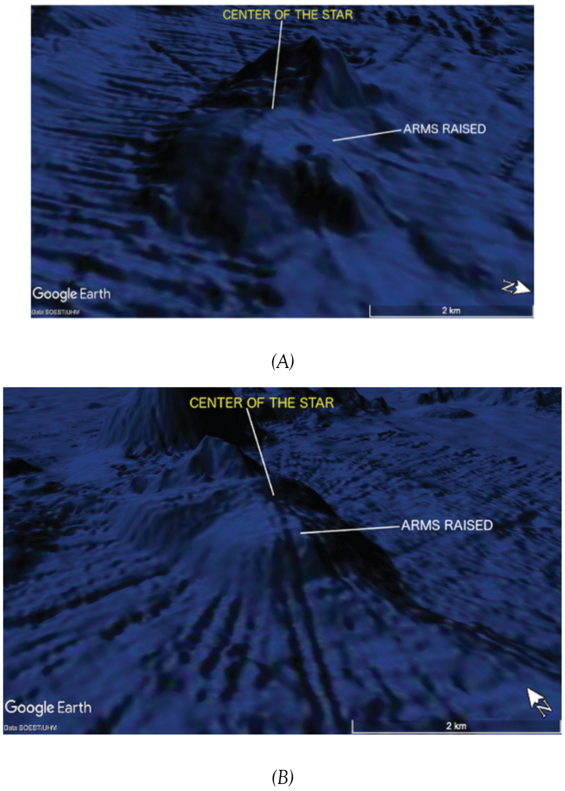

Figure 23) *Small stars with rising arms upward. A) Case 1. B) Case 2*

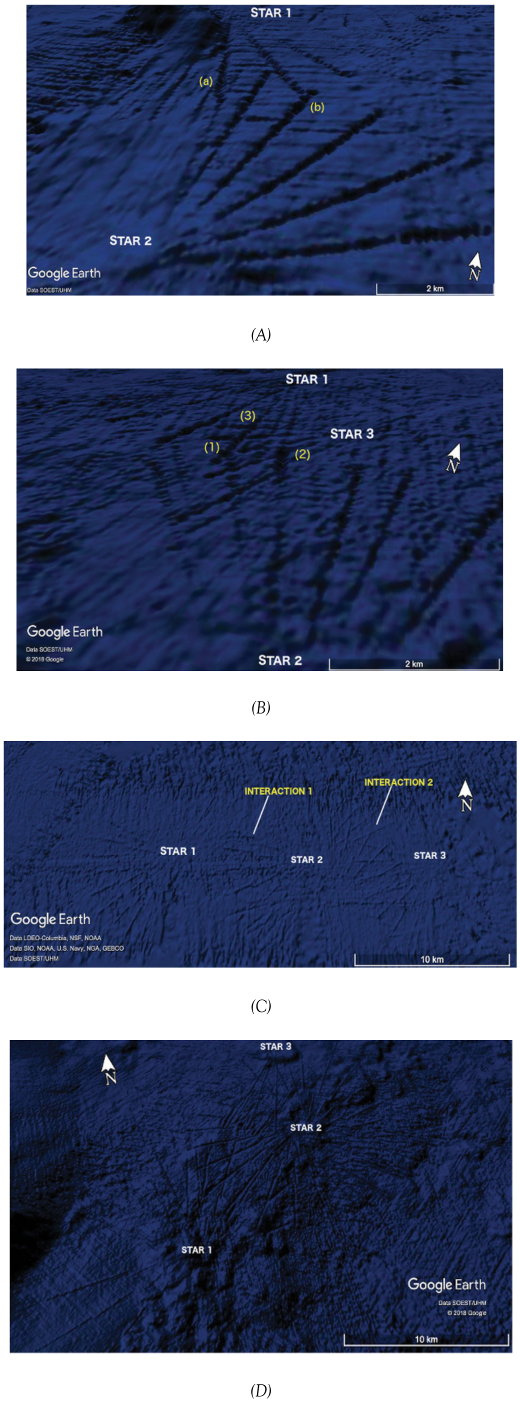

Figure 24) *Interactions between groups of small-scale stars. With Star 1, Star 2 and Star 3 the convergence zones of the arms of the respective stars have been indicated. A) Arm interactions [indicated with (a) and (b)] of two pockmark stars. It should be noted that in (a) there is a perfect overlap of the two arms which generate a deepening of the fracture. B) Arm interactions of three pockmark stars: (1) Star 1 - Star 2 interaction; (2) Star 1 - Star 2 interaction with the two arms merging into a single deeper arm; (3) Star 3 - Star 1 interaction. C-D) Multiple interactions between the arms of three stars that dislocate each other*

while there is an increase in activity in the Hawaiian offshore areas. This pulsating mechanism is believed to have been a feature that has accompanied the development of the Hawaiian Islands.

Observing the geological map of the Hawaiian Islands (21), which shows the main axes of rift in the different islands (https://pubs.usgs.gov/sim/2004/2824/SIM-2824_map.pdf), it is possible to notice some recurring geometries that characterize the islands present in the hotspot areas. In particular, the black dotted lines indicate axis of volcanic rift zone. The perfectly radial distribution of the axes can be seen in correspondence with

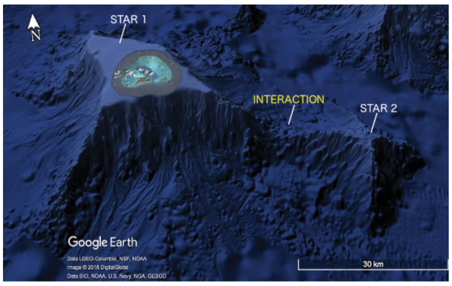

(A)

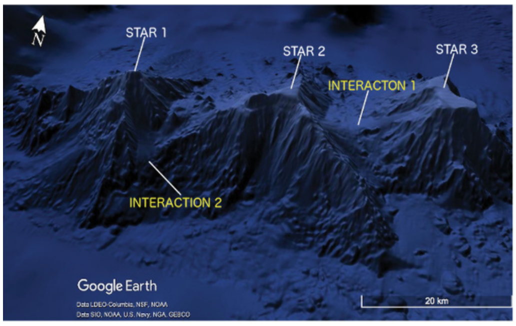

(B)

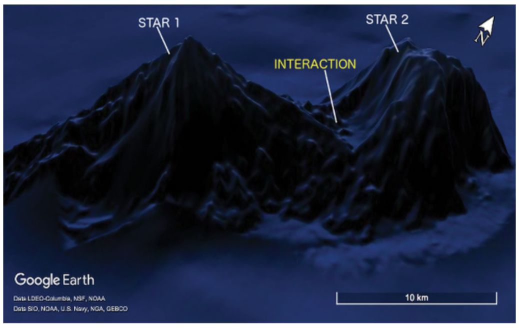

(C)

(D)

Figure 25) *Interactions between groups of medium-scale stars. A) Interaction between a pair of stars with the presence of a depression in the area where the two arms meet. B) Double interaction between the overlapping arms of three stars. C) Interaction between two stars, with the star 1 causing a landslide in the slope of the star 2. D) View from above of the previous image. It can be noted that the arm of the star 1 is deformed by the interaction with the star 2*

the former volcanic island indicated by Tmuf [upper left corner]. The two Kaua'i and Ni'ihau islands also have a star-like distribution of the rift axes which, in relation to their contiguous position, tend to overlap. The same interaction phenomenon occurs between the island of Ni'ihau and Ka'ula. Moving to the southernmost sector, it is possible to observe the same geometry in the islands with the largest extension [O'ahu, Moloka'i, Maui and Hawai'i] even if the regularity and symmetry of the structures seems to be less marked. In Figure 18 A a top view of the rift system present in the islands Ka'úla, Ni'ihau and Kaua'i [extracted from the map of the Hawaiian Islands (21)] showing a radial distribution of the rift axes. In Figure 18 B a close- up image of the active rift between the island of Ka'ula and Ni'ihau which, as they expand, tends to overlap their effects. Figure 19 shows the pattern of the rift zones associated with the volcanoes on the island of Hawai'i.

The observed radial structures tend to replicate at different scales: from small scale shapes with arm lengths in the 4-12 Km range, to medium-sized stars [from 50 to 150 km] highlighted by the rift axes belonging to the different islands of the chain of Hawaii, up to the big star of the Hawaiian islands, with the arm's length up to 500 Km. The peculiarity of these structures is that their morphological regularity and symmetry decrease with increasing size. This phenomenon can be due to several reasons:

i. The sphericity of the earth which, as the length of the arms increases, tends to curve straight propagation.

ii. The anisotropic nature of the earth's crust which tends to show its nonlinear influence as the length of the discontinuities increases.

iii. The presence of nearby rift that can alter the normal development of the shear zone associated with the single star.

In larger stars, such as the island of Hawai'i and Maui, the lithostatic load [volcanic building] that develops progressively exerts a mechanical stress that tends to modify the pressure conditions inside the underlying magma chambers. In this way the variation of the stress field can modify the prevailing development direction of the rift and, in more extreme cases, generate discordant tectonic discontinuities with the previous ones. Figure 20 shows an example of the interaction between uplift of Hawaiian Swell [light gray] and submergence along Hawaiian Ridge [dark gray], favoring eastward growth of long submarine ridges in front of hotspot magmatic locus (17).

CONCLUSION

The swelling of the hotspot zones that occurs in different areas of the world could explain the particular radial distribution of structural elements found in Hawaii.

The statistical analysis showed a correlation between the alignment direction, the type and the density of the structural elements: in some directions there is a marked concentration of structural elements of different types [for example, submarine ridge and/or bands of pockmarks and volcanic dikes] while in other directions there is total absence. This phenomenon could indicate directionality of the deformation linked to the shape of the underlying magmatic body. All the structural elements found in the seabed of the Hawaiian Islands have different points in common:

i. Converge at the most advanced part of the Hawaiian Islands

ii. Indicate, explicitly or implicitly, the existence of deep tectonic structures

The evolutionary pattern of the "big star" is very similar to that of the small-scale pockmark stars, which have colonized the seabed surrounding the Hawaiian Islands (7). The first phase concerns the presence of a magmatic underplating due to a flattened magmatic body pancake-shaped in which much rock is hot but solid and other rock is molten. The buoyancy causes a swelling, a classic phenomenon found in many areas of hotspot, with the formation of radial fractures that expand for hundreds of kilometers from the area of maximum curvature. The arms of this big star allow the ascent of the deep magma that generates linear eruptions in the seabed, with different intensities and characteristics depending on the direction. In the second phase there is the detachment, synchronous or asynchronous, of one or more plumes from the source that are stationed a few kilometers inside the crust: in this way more local swells are created with a much smaller extension than the initial one. The result is the presence of several volcanically active stars on which the main Hawaiian volcanoes develop.

The presence of radial rift systems associated with different volcanoes belonging to the Hawaiian Islands suggests that the process of star formation, observed at small scales (7) (Figure 21), also reproduced in the medium (Figure 22) and large scales (Figure 3). The constructive phase of the volcanoes due to the effusive activity [pre-shield, shield, post-shield and rejuvenation phases] is associated with the active thrust, produced by the underlying plume, which raises the pre-existing flat star (Figure 21) creating a singular correspondence three-dimensional (Figure 22). This interference between large-scale swelling [subcrustal pancake intrusion] and localized lift [plume detachment] (Figure

20) is evidenced by the presence of fractures and pockmarks that rise up the slope, which separates the bench from the oceanic area (Figure 4C), showing similarity with the structures pockmark-based developed towards the top of lava domes (Figures 23A and 23B).

The development of the volcano determines, in addition to the construction phases, also destructive phases, with the collapse of entire portions of the building that slide towards the sea areas, also favored by the movements of the rift zones. The phenomena of active rift that push the flanks of some Hawaiian volcanoes, for tens of kilometers towards the sea (13,14) and the collapse of entire portions of the volcanic structure are highlighted by experimental data and recent studies (14,23).

The grouping of several volcanic buildings characterized by radial symmetry rift axes shows a surprising similarity with the small-scale gregarious forms present in the Hawaiian offshore. In Figures 24A- D it is possible to observe clusters of small stars present in the Hawaiian seabed that generate conspicuous strike-slip dislocations between their arms, due to the contiguous position. The same phenomenon can also be observed directly at medium scales: in addition to the already mentioned phenomena of interference between the prolongation of the Mauna Kea volcano [Hilo Ridge] with that of the Kohala volcano (17) and the interactions between the radial rift of the Kaua'i islands, Ni'ihau and Ka'ula (Figures 18 A and 18 B) also exist potential future interactions. We refer in particular to the possible interactions between the active rift, Puna Ridge and Hilo Ridge, relative to the flanks of the volcano Kilawea and Mauna Loa (Figure 2).

The historic eruption and earthquake catalogues confirm the existence of a synchronism between seismic and volcanic activity of the radial rift systems of Hawaiian volcanoes, located a short distance from each other. In particular earthquakes in the Kaoiki area occur in sequence with eruptions from the NERZ [Northeast Rift Zone], and earthquakes in the Kona and Hilea areas occur in sequence with eruptions from the SWRZ [Southwest Rift Zone] (19).

We must however consider that the interactions between contiguous stars and the greater crust heterogeneity have conditioned the development and the morphology of each star, reducing the degree of symmetry. This tectonic process, based on a recursive phenomenon of plume detachment starting from a pancake-like subcrostal magmatic body, is able to generate star-like structures at different scales. Scale invariance, in particular physico-chemical conditions, allows to replicate tectonic morphologies with a radial structure, regardless of the scale considered and can extend to phenomena closely related to the main one. We refer to the clustering and interaction between groups of contiguous stars that have been described both at small (Figures 24A-D) and medium scales (Figures 25A-D). These last images refer to the submerged volcanoes (seamount and tablemount) of the Hawaii-Emperor chain, which show a marked radial structure and interactions between the respective flanks that, on several occasions, can produce the landslide of entire slopes.

The big star of Hawaii, highlighted by the tectonic structures developed up to 500 km lengths and the swelling found in over fifty hotspots (22,23), due to the buoyancy of the magmatic underplating, suggest that the interaction between tectonic stars, consistently as found on the small stars, it is also a common phenomenon on large scales. A mechanism of this kind could therefore reveal, in the coming years, a marked influence on the tectonic-volcanic phenomena of large sectors of our planet.

For supplementary information about pockmark stars with a full image collection, visit:

https://www.slideshare.net/RobertoSpina2/the-big-starofhawaiianislands

ACKNOWLEDGMENT

Thanks to Martina Spina for the realization of the tectonic schemes of Figure 17.

REFERENCES

1. Hovland M, Gardner JV, Judd AG. The significance of pockmarks to understanding fluid flow processes and geohazards. Geofluids. 2002;2:127-36.
2. Pinet N, Duchesne M, Lavoie D. Linking a linear pockmark train with a buried Palaeozoic structure: a case study from the St. Lawrence Estuary. Geo-Mar Letter. 2010;30:517-22.
3. Pilcher R, Argent J. Mega-pockmarks and linear pockmark trains on the West African continental margin. Mar Geol. 224:15-32.
4. Li J, Shenghe W, Jiajia Z, et al. Seafloor pockmarks and linear pockmark trains linked to buried turbiditic palaeo-channel in the niger delta basin, West African. International Conference and Exhibition, Melbourne, Australia. 2015:81-81.
5. Barrie JV, Hill PR. Holocene faulting on a tectonic margin: Georgia Basin, British Columbia, Canada. Geo-Mar Letter. 2004;24:86-96.
6. Forwick M, Baeten NJ, Vorren TO. Pockmarks in spitsbergen fjords. Norw J Geol. 2009;89:65-77.
7. Spina R. The pockmark stars: radial structures in the seabed surrounding the Hawaii Islands. J Environ Geol. 2017;1(1);33-50.
8. King SD, Adam C. Hotspot swells revisited. Phys Earth Planet. 2014;235:66-83.
9. Crough ST. Thermal origin of mid plate hot-spot swells. Geophys J R Astro Soc. 1978;55;451-79.
10. Holcomb RT, Holmes M, Denlinger RP, et al. Submarine hawaiian north arch volcanic field. EOS. 1988;69:1445.
11. Lipman PW, Calvert AT. Early growth of Kohala volcano and formation of long Hawaiian rift zones. Geology. 2011;39(7):659-62.
12. Fiske RS, Jackson ED. Influence of gravitational stresses on the orientation and growth of Hawaiian volcanic rifts [abs.]. Geological Society of America Abstracts with Programs. 1972;4(3):157.
13. Denlinger RP, Morgan JK. Instability of Hawaiian Volcanoes. U.S. Geological Survey Professional Paper. 2014:1801.
14. Swanson DA, Duffield WA, Fiske RS. Displacement of the south flank of Kilauea volcano; the result of forceful intrusion of magma into the rift zones. U.S. Geological Survey Professional Paper. 1976;963:39.
15. Leslie SC, Moore GF, Morgan JK. Internal structure of Puna Ridge: evolution of the submarine East Rift Zone of Kilauea Volcano, Hawai'i. J Volcanol Geotherm Res. 2004;129:237-59.
16. Johnson KTM, Ren ZY, Takahashi E. Rift zone magmatism at Puna and Hana Ridges, Hawaii. Goldschmidt Conference Abstracts. 2003:A191.
17. Lipman PW, Calvert AT. Early growth of Kohala volcano and formation of long Hawaiian rift zones. Geology. 2011;39:659-62.
18. Holcomb RT, Nelson BK, Reiners PW, et al. Overlapping volcanoes: The origin of Hilo Ridge, Hawaii. Geology. 2000; 28:547-50.
19. Walter TR, Amelung F. Volcano-earthquake interaction at Mauna Loa volcano, Hawaii. J Geophys Res. 2006;111:B05204.
20. http://www.yongtechnology.com/download/georose.
21. Holcomb RT, Robinson JE. Maps of Hawaiian islands exclusive economic zone interpreted from GLORIA Sidescan-Sonar Imagery. U.S. Geological Survey 2004.
22. Crough ST. Thermal origin of mid plate hot-spot swells. Geophys J R Astro Soc. 1978;55:451-79.
23. Moore JG, Clague DA, Holcomb RT, et al. Prodigious submarine landslides on the Hawaiian Ridge. J Geophys Res. 1989;94:465-17.